Cranfield

College of Aeronautics Report No.9112
August 1991

Some aspects of shock capturing methods for gas dynamics

E.F.Toro

Department of Aerodynamics and Fluid Mechanics
College of Aeronautics
Cranfield Institute of Technology
Cranfield, Bedford MK43 0AL. England

Cranfield

College of Aeronautics Report No.9112
August 1991

Some aspects of shock capturing methods for gas dynamics

E.F.Toro

Department of Aerodynamics and Fluid Mechanics
College of Aeronautics
Cranfield Institute of Technology
Cranfield, Bedford MK43 0AL. England

Paper presented at the Computational Fluid Dynamics Workshop July 1991
Shoch Wave Research Center
Institute of Fluid Science
Tohoku University
Sendai, Japan

ISBN 1 871564 32 8

£8.00

ABSTRACT

Three topics on modern shock capturing methods for the time-dependent Euler equations of Gas Dynamics are addressed. First we present the Weighted Average Flux Method (or WAF), one of several Riemann-problem based shock capturing methods. Then we deal with the Riemann problem. We present an efficient exact Riemann solver, a robust non-iterative Riemann solver based on the behaviour of the exact solver, and an improved version of the Harten-Lax-van Leer Riemann solver . Also, a very simple linearised Riemann solver is presented together with a Riemann solver adaptation procedure. We also present a Riemann-solver adaptation procedure that has proved successful. Applications of the WAF method with the various Riemann solvers are presented.

1. INTRODUCTION.

A significant contribution to the current state of modern Computational Fluid Dynamics (CFD) has come via Riemann-problem based, or Godunov-type, numerical methods. These are extensions of the first-order accurate method of Godunov (1959). Riemann-problem based methods (or RP methods for short) are directly applicable to time-dependent one-dimensional systems of hyperbolic conservation laws or to two-dimensional systems that are hyperbolic in a time-like variable (e.g. the two-dimensional steady supersonic Euler equations). Extensions of these methods to multidimensional problems is carried out via the finite volume method coupled with one-dimensional physics in the direction normal to the control volume interface.

Many workers have contributed to the development of RP methods; outstanding examples are Godunov (1959), van Leer (1979), Roe (1981), Harten (1983), Osher (1984).

RP methods use the solution of the Riemann problem with data in volumes

(i,i+1) to define an intercell numerical flux $F_{i+1/2}$ to be used in the conservative, explicit formula

$$U_i^{n+1} = U_i^n - \frac{\Delta t}{\Delta x} (F_{i-1/2} - F_{i+1/2})$$

The various RP methods differ in the definition for the intercell flux $F_{i+1/2}$, in the way the local Riemann problem solution is used and in the way higher accuracy without the spurious oscillations of traditional methods is achieved.

The weigthed average flux (WAF) approach for systems of hyperbolic conservation laws was presented by Toro (1989a). This method achieves second-order accuracy using the conventional piece-wise constant data Riemann problem. Also, it is sufficiently flexible to accept virtually any approximation to the solution of the local Riemann problem as well as the exact solution . This second feature can be be taken advantage of by, for example, constructing a hierarchy of Riemann solvers to be used in an adaptive Riemann solver fashion.

The WAF method has been applied to a variety of realistic flow situations (Toro,1989b, 1991). The experience gained in the exercise has resulted in further developments and useful simplifications to the technique. In this paper we present the method as applied specifically to the Euler equations in one and two space dimensions. An efficient exact Riemann solver as well as a variety of approximate Riemann solvers that can be used with WAF are presented.

The paper is organized as follows: In section 2 the WAF method is presented; section 3 deals with Riemann solvers; in section 4 we present numerical results and conclusions are drawn in section 5.

2. THE WEIGHTED AVERAGE FLUX METHOD (WAF)

For the purpose of this section we shall restrict ourselves to the time-dependent one-dimensional Euler equations written in conservation form, namely

$$U_t + [F(U)]_x = 0 \qquad (1)$$

Here U is the vector of conserved variables and F(U) is the vector of the

corresponding fluxes, i.e.

$$U = \begin{bmatrix} \rho \\ \rho u \\ E \end{bmatrix}, \quad F = \begin{bmatrix} \rho u \\ \rho u^2 + p \\ u(E+p) \end{bmatrix} \tag{2}$$

The conserved variables are: the density ρ, the momentum ρu, where u is the velocity, and the total energy E, where $E = \frac{1}{2}\rho u^2 + \rho e$ with e denoting the specific internal, or intrinsic, energy.

The symbols t and x denote time and space and are the independent variables. The associated subscripts in Eq.(1) denote partial differentiation. Note that there are more dependent variables than there are equations and thus a closure condition is required. We take the ideal gas equation of state as the closure condition, namely

$$e = e(\rho, p) = \frac{p}{(\gamma - 1)\rho} \tag{3}$$

with γ denoting ratio of specific heats.

The Euler equations have discontinuous solutions (shock waves, contacts) and it is therefore more appropriate to recast the differential equations (1) in integral form as

$$\oint [U dx - F(U) dt] = 0 \tag{4}$$

2.1 DESCRIPTION OF THE WAF METHOD.

Consider a domain in the x-t plane discretised by a grid of dimensions Δx_i and Δt as shown in Fig.1. Evaluation of the integral (4) around cell i produces

$$U_i^{n+1} = U_i^n - \frac{\Delta t}{\Delta x_i} \left[F_{i+1/2} - F_{i-1/2} \right] \tag{5}$$

with suitable interpretations for the the discrete values of the conserved variables and fluxes. This explicit conservative formula gives a time-marching scheme in terms of the data U_i^n, the grid dimensions and the intercell fluxes $F_{i+1/2}$ and $F_{i-1/2}$. The notation U_i^n means the discrete value of U in cell i at time level n. For convenience, we often omit the superscript n.

The scheme (5) is completely defined once the fluxes have been specified. Let us consider $F_{i+1/2}$. The WAF method assumes that all conserved variables have a piece-wise constant distribution in x at any time level n. Locally, two neighbouring constant states (U_i, U_{i+1}) are the initial data for the relevant differential (or integral) equations. This initial value problem is known as the *Riemann problem.* In general, this local problem is simpler to solve than the global problem. The global solution can be constructed by using the sequence of local Riemann problems {RP(i,i+1)} in a variety of ways, depending on the particular method in use. The solution of the Riemann problem for the unsteady one-dimensional Euler equations (1), when represented on the x-t plane, looks as depicted in Fig.2. There are three waves. The middle wave is always a contact discontinuity. The left and right waves are called the acoustic waves and can be either shocks or rarefactions. Contacts and shocks are discontinuities, rarefaction waves are continuous solutions. We shall denote the solution of the Riemann problem with data U_i and U_{i+1} by $U^*(x/t, U_i, U_{i+1})$ or simply by $U^*(x/t)$. It is only a function of the similarity variable x/t. Note that we centre the Riemann problem at the origin (0,0) in the x-t plane.

Godunov (1959) is credited with being the first to use the solution of the local Riemann problems to evaluate the numerical intercell flux $F_{i+1/2}$ in (5). Godunov's flux is given by

$$F^{GOD}_{i+1/2} = F[U^*(0,U_i,U_{i+1})] \qquad (6)$$

Note that $U^*(0,U_i,U_{i+1})$ is constant for $t > 0$. The density (and thus the internal energy and the temperature) is constant in between the waves with discontinuous jumps across shocks and contacts. The structure of the solution of the Riemann problem contains therefore four constant states: U_i (left state data), U^*_L (left of contact), U^*_R (right of contact) and U_{i+1} (right state data). Special care is needed in the case when the value $x/t = 0$ lies inside a rarefaction fan (sonic flow). The Godunov Method is only first-order accurate and is therefore too inaccurate to be used in practice.

The WAF Method is a second-order extension of Godunov's Method. Higher accuracy is achieved by simply defining the inter cell flux $F_{i+1/2}$ as an integral average of the flux function F(U) in (1) evaluated at the solution

$U^*(x/t)$ of the Riemann problem with data U_i, U_{i+1} at time $t = \frac{1}{2}\Delta t$.

Suppose the neighbouring cells i and i +1 have spacings Δx_i and Δx_{i+1}, then the WAF flux is

$$\left.\begin{aligned} F^{WAF}_{i+1/2} &= \frac{1}{-2x_1}\int_{x_1}^{0} F(U^*)dx \;+\; \frac{1}{2x_2}\int_{0}^{x_2} F(U^*)dx \\ x_1 &= -\Delta x_i/2 \quad ; \; x_2 = \Delta x_{i+1}/2 \end{aligned}\right\} \qquad (7)$$

where $U^* = U(x/\Delta t/2)$ is the solution of the Riemann problem with data U^n_i, U^n_{i+1} at time $\Delta t/2$. The integration in (7) goes from the centre of the left cell i to the centre of the right cell i+1 at time $t = \Delta t/2 =$ constant. A simpler expression results by choosing $x_1 = -\frac{1}{2}\min\left\{\Delta x_i, \Delta x_{i+1}\right\}$, $x_2 = \min\left\{\Delta x_i, \Delta x_{i+1}\right\}$.

The integration can be made as accurate as desired, but the presence of rarefaction fans makes it more complicated, which for practical applications is undesirable. Experience has indicated to us that acknowledging fans is only important in the presence of sonic flow, that is when one of the acoustic waves is a rarefaction centred around the t-axis, and even in this case one may simplify the wave structure somewhat, as we shall explain later. In any event, we assume that the solution of the Riemann problem has N waves with N associated wave speeds λ_k. For simplicity let us consider the regular grid case with $\Delta x_i = \Delta x_{i+1} = \Delta x$. The Courant numbers ν_k associated with the wave speeds λ_k are

$$\nu_k = \lambda_k/(\Delta x/\Delta t) \qquad (8)$$

The WAF flux can then be written as

$$F_{i+1/2} = \sum_{k=1}^{N+1} W_k F^{(k)}_{i+1/2} \qquad (9)$$

where the coefficients W_k (or weights) are the geometric extents of the constant states in the integral (7). $F^{(k)}_{i+1/2}$ is the flux function F in (1) evaluated at the solution of the Riemann problem in region k. Fig.3 illustrates the situation. It is easy to see that the weights W_k can be written in terms of the Courant numbers ν_k as follows

$$\left.\begin{aligned} W_k &= \tfrac{1}{2}(\nu_k - \nu_{k-1}) \\ \nu_0 &= -1 \text{ and } \nu_{N+1} = +1 \end{aligned}\right\} \qquad (10)$$

Note that $W_k \geq 0$ for all k and that $\sum_{k=1}^{N+1} W_k = 1$.

Clearly $F^{WAF}_{i+1/2}$ gives an extension of the first-order Godunov Method, for if $W_K = 1$ and $W_k = 0$ for all $k \neq K$ in (9) $F^{WAF}_{i+1/2}$ reproduces the Godunov flux. The region K is that associated with $x/t = 0$. The wave structure of the local Riemann problem RP(i,i+1) determines which weight corresponds to the Godunov's Method. For instance, if the flow is fully supersonic i.e. $\lambda_1 > 0$ then W_1 is the Godunov's weight. If the local flow is fully subsonic ($\lambda_3 < 0$) then the Godunov's weight is W_4, etc. The case of t-axis centred expansion fans will be dealt with later when discussing solutions of the Riemann problem.

The Godunov's weight represents the upwind bias of the WAF scheme and controls stability. All other weights represent downwind contributions; they increase accuracy. When applied to the model hyperbolic equation

$$u_t + a u_x = 0 \ , \ a = \text{constant} \qquad (11)$$

the WAF method reduces identically to the Lax-Wendroff method and it is therefore, for this model equation, second order accurate in space and time. For non-linear hyperbolic systems the numerical results are like those obtained by typical second-order accurate methods.

A disadvantage of the added accuracy of the WAF scheme is that spurious oscillations near high gradients are produced. This is in accordance with the well known Godunov's theorem (Godunov, 1959). An oscillation free version of the method will be presented in the following section. This is different from

that given in the original paper (Toro, 1989a) and simpler to implement in practice..

As observed in the paper by Toro (1989b) the WAF flux can be expressed, after using (10) in (9), as

$$F^{WAF}_{i+1/2} = \frac{1}{2}\left[F_i + F_{i+1}\right] - \frac{1}{2}\sum_{k=1}^{N} \nu_k \Delta F^{(k)}_{i+1/2} \tag{12}$$

where

$$\Delta F^{(k)}_{i+1/2} = F^{(k+1)}_{i+1/2} - F^{(k)}_{i+1/2} \tag{13}$$

is the flux jump across wave k.

Formulae (12)-(13) are more revealing. In particular, they expose the flux-difference splitting character of the method. Also, expression (12) makes it easier to compare the similarities and differences of the WAF method with those of other modern methods, such as Roe's method (Roe, 1981)

An alternative formulation of the WAF method is

$$F^{WAF}_{i+1/2} = F(\bar{V}_{i+1/2}) \tag{14}$$

where $\bar{V}_{i+1/2}$ is obtained by replacing the flux F in (9) by an actual state V. There are at least two choices for V, namely the vector of primitive variables (ρ,u,p) or the vector of conserved variables $(\rho,\rho u,E)$. In either case the average state can be written as

$$\bar{V}_{i+1/2} = \frac{1}{2}\left[V_i + V_{i+1}\right] - \frac{1}{2}\sum_{k=1}^{N} \nu_k \Delta V^{(k)}_{i+1/2} \tag{15}$$

where

$$\Delta V^{(k)}_{i+1/2} = V^{(k+1)}_{i+1/2} - V^{(k)}_{i+1/2} \tag{16}$$

is the jump in V across the wave k and $V^{(k)}_{i+1/2}$ is the value of V in region k.

From the point of view of computational efficiency, formulae (14) - (16) are more attractive than (12) - (13); there are fewer operations involved. Numerical experiments show that the results of these two formulations are virtually indistinguishable. The same remark applies to the choice of variables for the states V in (14) - (16). From a theoretical point of view it is of interest to note that if the state V in (15) represents the conserved variables then this formulation of the WAF method makes it analagous to the Richtmyer-Morton method , or two-step Lax-Wendroff method as it is sometimes called, where

$$\bar{V}_{i+1/2} = \frac{1}{2}\left[V_i + V_{i+1}\right] - \frac{1}{2}\frac{\Delta t}{\Delta x}\left[F_{i+1} - F_i\right] \qquad (17)$$

This can be immediately seen by integrating the conservation laws (1), or (4), in the rectangle

$$-\frac{1}{2}\Delta x \le x \le \frac{1}{2}\Delta x \ , \ 0 \le t \le \frac{1}{2}\Delta t$$

As a point of interest it is worth remarking that formulation (15) - (16) of WAF, under certain special circumstances, may lead to entropy violating solutions (rarefaction shocks). This depends entirely on the solution of the Riemann problem and will be addressed later.

4.2 TVD VERSION OF THE WAF METHOD.

Given the second-order character of the WAF method spurious oscillations near high gradients are expected. In the original paper (Toro, 1989a) it was demonstrated that an oscillation-free version of WAF based on the flux-limiter concept can be constructed. In this paper we present an alternative interpretation of the oscillation-free method. Strictly speaking both oscillation-free versions are mathematically equivalent, but the present formulation has some computational advantages, the resulting scheme is neater and coding is significantly simpler.

We follow Toro (1989d), where a detailed oscillation-free construction for a model equation was carried out. Consider the linear advection equation $u_t + au_x = 0$. Unless otherwise stated we shall assume that the constant speed a is positive. Here u is the conserved quantity and F(u) = au. At this stage

we introduce the concept of total variation of a discrete solution $\{u_i^n\}$. The total variation of the solution at time level n, denoted by $TV(u^n)$, is defined as

$$TV(u^n) = \sum_i | u_{i+1}^n - u_i^n | \qquad (18)$$

Note that this is essentially a measure of the oscillatory character of the solution.

A large class of useful difference schemes are those whose total variation diminishes with time, i.e.

$$TV(u^{n+1}) \leq TV(u^n)$$

Such schemes are called total variation diminishing schemes, or TVD schemes for short (Harten, 1983).

In order to apply WAF to eqn.(11) the Riemann problem for (11) must be solved. If the initial data at time level n for the local Riemann problem RP(i,i+1) centred at $x_{i+1/2}$ is $u(t^n,x) = u_i^n$ if $x < x_{i+1/2}$ and $u(t^n,x) = u_{i+1}^n$ if $x > x_{i+1/2}$ then the solution is trivial and can be written as

$$u(x,t) = \begin{cases} u_i^n, & \text{if } (x-x_{i+1/2})/t < a \\ u_{i+1}^n, & \text{if } (x-x_{i+1/2})/t > a \end{cases} \qquad (19)$$

Having solved the local Riemann problem RP(i,i+1) we can now evaluate the intercell flux $F_{i+1/2}$. To this end it is instructive to use definition (9) for $F_{i+1/2}$. Since we are considering the case $a > 0$, the upwind (or upstream) region lies to the left of the characteristic line $dx/dt = a$ and the downwind (or downstream) region lies to the right of $dx/dt = a$. The respective normalised lengths associated with these regions are the weights

$$W_1 = \tfrac{1}{2}(1+\nu), \quad W_2 = \tfrac{1}{2}(1-\nu) \qquad (20)$$

where $\nu = a\Delta t/\Delta x$ is the Courant number associated with the wave speed a. Fig. 4 illusttrates the meaning of the weights.

The intercell flux $F_{i+1/2}$ becomes

$$F_{i+1/2} = \frac{1}{2}(1+\nu)au_i^n + \frac{1}{2}(1-\nu)au_{i+1}^n \qquad (21)$$

which is effectively a weighted average of the upwind and downwind parts of the solution of the local Riemann problem. Note that $W_1 + W_2 = 1$ and that $W_1, W_2 \geq 0$. If $W_1 = 1$ and $W_2 = 0$ the flux (21) gives the Godunov's method (first order upwind); if $W_1 = 0$ and $W_2 = 1$ the flux (21) gives a downwind method, which is unstable. The upwind method is stable but very inaccurate. If the weights in eqn.(21) are unaltered then the Lax-Wendroff method results; this is second-order accurate in space and time. In a sense the flux (21) is an average between a stable and an unstable scheme. The weight W_1 (upwind) controls stability and the weight W_2 (downwind) gives higher accuracy.

It is the inherent higher accuracy of the scheme given by (21) what produces the spurious oscillations near high gradients. In what follows we present a mechanism for eliminating the spurious oscillations.

2.2.1 TVD REGIONS AND WAVE-SPEED AMPLIFIERS

In the presence of high gradients or oscillatory data we need to reduce the role of the downwind weight W_2 and increase that of the upwind weight W_1. This can be accomplished by altering the wave speed a (see Fig. 4) via an amplifying function A still to be found. Set $\bar{a} = Aa$. The modified Courant number becomes

$$\bar{\nu} = \frac{Aa\Delta T}{\Delta x} = A\nu \qquad (22)$$

The modified flux (21) becomes

$$F_{i+1/2} = \frac{1}{2}(1+\bar{\nu})au_i^n + \frac{1}{2}(1-\bar{\nu})au_{i+1}^n$$

or, as in eqn.(12) with N=1 for the intercell flux

$$F_{i+1/2} = \frac{1}{2}\left(au_i^n + au_{i+1}^n\right) - \frac{1}{2}\bar{\nu}\left(au_{i+1}^n - au_i^n\right) \tag{23}$$

In order to find the amplifying function A in eqn.(22) we consider first the case of positive speed a. Two obvious bounds for A are given by the fully upwinding case ($\bar{\nu} = 1$, $\bar{W}_1 = 1$, $\bar{W}_2 = 0$) and the fully downwinding case ($\bar{\nu} = -1$, $\bar{W}_1 = 0$, $\bar{W}_2 = 1$). Thus we choose A such that

$$-\frac{1}{\nu} \le A \le \frac{1}{\nu} \tag{24}$$

Substitution of the modified intercell fluxes $F_{i+1/2}$ and $F_{i-1/2}$ according to eqn.(23) into the conservative scheme (5) gives

$$u_i^{n+1} = u_i^n - \frac{1}{2}\nu\left\{\left(u_{i+1}^n - u_{i-1}^n\right) + \nu\left[A_{i+1/2}\left(u_i^n - u_{i+1}^n\right) - A_{i-1/2}\left(u_{i-1}^n - u_i^n\right)\right]\right\} \tag{25}$$

On division through by $u_{i-1}^n - u_i^n$ and rearranging

$$\frac{u_i^{n+1} - u_i^n}{u_{i-1}^n - u_i^n} = \frac{1}{2}\nu^2\left[\frac{1}{r_i}\left(\frac{1}{\nu} - A_{i+1/2}\right) + A_{i-1/2} + \frac{1}{\nu}\right] \tag{26}$$

with

$$r_i = \frac{u_i^n - u_{i-1}^n}{u_{i+1}^n - u_i^n} \tag{27}$$

The "flow parameter" r_i is the ratio of the upwind change to the local change in the conserved variable u.

A simple sufficient condition for avoiding overshoots or new extrema is

$$0 \le \frac{u_i^{n+1} - u_i^n}{u_{i-1}^n - u_i^n} \le 1 \tag{28}$$

That is to say, the new value u^{n+1} lies between the data values u_{i-1}^n and u_i^n. From equations (26) and (28) it follows that

$$0 \le \frac{1}{2}\nu^2\left[\frac{1}{r_i}\left(\frac{1}{\nu} - A_{i+1/2}\right) + A_{i-1/2} + \frac{1}{\nu}\right] \le 1 \qquad (29)$$

or

$$-\frac{1}{\nu} \le \frac{1}{r_i}\left(\frac{1}{\nu} - A_{i+1/2}\right) + A_{i-1/2} \le \frac{2-\nu}{\nu^2} \qquad (30)$$

It is convenient to re-state the constraint given by the inequalities (24) as

$$L \le A_{i\pm1/2} \le \frac{1}{\nu} \text{ , with L in } \left[-\frac{1}{\nu},1\right] \qquad (31)$$

If $A \equiv 1$ the original scheme is unchanged. If $A > 1$ then A is strictly an amplifying function. In the analysis that follows we shall also admit the possibility of reducing the wave speed, that is to say of increasing the role of the downwind part of the scheme. The lower bound L in (31) is now open to choice within the interval $\left[-\frac{1}{\nu}, 1\right]$.

The problem is to choose amplifying functions $A_{i\pm1/2}$ so that both inequalities (30) - (31) are simultaneously satisfied. This can be achieved by taking

$$-S_L \le \frac{1}{r_i}\left[\frac{1}{\nu} - A_{i+1/2}\right] \le S_R \qquad (32)$$

$$-\frac{1}{\nu} \le L \le A_{i\pm1/2} \le \frac{1}{\nu} \qquad (33)$$

with

$$S_L = L + 1/\nu \text{ , } S_R = 2(1-\nu)/\nu^2 \qquad (34)$$

The analysis leading to (32) - (34) is based on the assumption that the speed a in the model equation (12) is positive. For negative a the result is identical but ν is replaced by $|\nu|$. Hence the general case is

$$-S_L \le \frac{1}{r_i}\left[\frac{1}{|\nu|} - A_{i+1/2}\right] \le S_R \qquad (35)$$

$$-\frac{1}{|\nu|} \le L \le A_{i\pm1/2} \le \frac{1}{|\nu|} \qquad (36)$$

with S_L and S_R redefined as

$$S_L = L + 1/|\nu| \ , \ S_R = 2(1-|\nu|)/|\nu|^2 \tag{37}$$

Now the main inequality (30) reads

$$-\frac{1}{|\nu|} \le \frac{1}{r_i}\left[\frac{1}{|\nu|} - A_{i+1/2}\right] + A_{i-1/2} \le \frac{2-|\nu|}{|\nu|^2} \tag{38}$$

Clearly, the choices (35) - (36) satisfy (38) automatically, whose bounds we now analyse. For convenience, we ignore subscripts of the functions A and the parameter r

From (35) $-S_L \le \frac{1}{r}\left[\frac{1}{|\nu|} - A\right]$. If $r > 0$ then $-S_L r \le \frac{1}{|\nu|} - A$ or

$$A \le A_L \ , \ A_L = \frac{1}{|\nu|} + S_L r \tag{39}$$

If $r < 0$ then

$$A \ge A_L \tag{40}$$

The upper inequality (38) gives

$$A \ge A_R \ , \ A_R = \frac{1}{|\nu|} - S_R r \ , \ \text{if } r > 0 \tag{41}$$

$$A \le A_R \ , \ \text{if } r < 0 \tag{42}$$

For $L > -1/|\nu|$ in (31) there are two TVD zones Z_L and Z_R on the r-A plane. These are shown in Fig. 5. The horizontal bounds are $A = L$ and $A = 1/|\nu|$. There are also two straight lines A_L and A_R with positive and negative slopes respectively. These lines are defined in eqns. (39) and (41).

The two TVD regions are, in set notation,

$$Z_L = \left\{(r,A) \text{ such that } r \le 0,\ A \ge A_L,\ L \le A \le 1/|\nu|\right\}$$

$$Z_R = \left\{(r,A) \text{ such that } r \geq 0,\ A \geq A_R,\ L \leq A \leq 1/|\nu|\right\}$$

For the case $L = -1/|\nu|$ the zone Z_L coalesce to the single line $A = 1/|\nu|$. This means that if $r \leq 0$ only upwind differencing is allowed in this special case.

2.2.2 CONSTRUCTION OF AMPLIFIERS

There are an unlimited number of choices for $A = A(r)$, where r is the flow parameter defined by eqn.(27). A simple way forward is to use the relationship that exists between our amplifiers A and flux limiters B. This is found in Toro (1989d).

$$A = \frac{1 - (1-|\nu|)B}{|\nu|} \tag{43}$$

There exists an enormous amount of experience in constructing and applying flux limiters B. We now profit from that experience and choose B directly to compute A in (43). A popular flux limiter is the so called MINBEE limiter with the associated A(r) given as

$$A_M = \begin{cases} 1/|\nu| & , r \leq 0 \\ [1 - (1-|\nu|)r]/|\nu| & , 0 \leq r \leq 1 \\ 1 & r \geq 1 \end{cases} \tag{44}$$

Another popular flux limiter is the so called SUPERBEE. The corresponding amplifying function is

$$A_S = \begin{cases} \dfrac{1 - 2(1-|\nu|)}{|\nu|} & r \geq 2 \\ \dfrac{1 - r(1-|\nu|)}{|\nu|} & 1 \leq r \leq 2 \\ 1 & \frac{1}{2} \leq r \leq 1 \\ \dfrac{1 - 2r(1-|\nu|)}{|\nu|} & 0 \leq r \leq \frac{1}{2} \\ 1/|\nu| & r \leq 0 \end{cases} \tag{45}$$

Alternatively, one can construct amplifiers directly. Various choices

were tested by Toro (1989d)

The most important requirement for a function A is its performance in problems other than the model equation $u_t + au_x = 0$, in particular for non-linear systems of hyperbolic conservation laws such as the Euler equations (1). This is the subject of the next section.

2.2.3 OSCILLATION-FREE PROCEDURES FOR SYSTEMS OF EQUATIONS

The procedures described in the previous section are, strictly speaking, valid only for the model equation $u_t + au_x = 0$. For decoupled linear systems linear systems the extension is trivial. The problem arises when dealing with non-linear systems such as the Euler equations. In this case the oscillation-free procedures are empirical.

Suppose we are solving the one dimensional Euler equations (1). There are three waves to take care of and consequently we must construct three amplifying functions A_k, one for each wave. Also, there are three fluxes, each one being affected by all three waves. Moreover, for the linear scalar case the argument r of A is itself a function of the conserved variable u (eq. 27).

Having computed A_k for each wave one then generalises (23) to the system case as follows.

$$F_{i+1/2} = \frac{1}{2}\left[F_i + F_{i+1}\right] - \frac{1}{2}\sum_{k=1}^{N} A_k \nu_k \Delta F^{(k)}_{i+1/2} \qquad (46)$$

Compare this oscillation free flux to the fully second-order flux (12). The modification is remarkably simple. If one chooses to use version (14) - (16) of WAF then the modified oscillation free averaged state $\bar{V}_{i+1/2}$ in (15) becomes.

$$\bar{V}_{i+1/2} = \frac{1}{2}\left[V_i + V_{i+1}\right] - \frac{1}{2}\sum_{k=1}^{N} A_k \nu_k \Delta V^{(k)}_{i+1/2} \qquad (47)$$

The computation of A_R for each wave k, is based on a flow parameter $r_i^{(k)}$ defined as follows:

$$r_i^{(k)} = \begin{cases} \dfrac{\Delta Q^{(k)}_{i-1/2}}{\Delta Q^{(k)}_{i+1/2}}, & \text{if } \nu_k > 0 \\ \dfrac{\Delta Q^{(k)}_{i+3/2}}{\Delta Q^{(k)}_{i+1/2}}, & \text{if } \nu_k < 0 \end{cases} \qquad (48)$$

where Q is a suitable flow variable. The density and the specific internal energy, or simply p/ρ , are good candidates.

In eq.(48) $\Delta Q^{(k)}_{i+1/2}$ is the jump in Q across wave k in the solution of the Riemann problem with data (U_i, U_{i+1}). We call $\Delta Q^{(k)}_{i+1/2}$ the <u>local jump</u>. The numerators in (48) are the <u>upwind jumps</u> in Q across the wave k. Their choice depends on the wave direction (sign of ν_k). The flow parameter $r_i^{(k)}$ in (48) is the ratio of the upwind to the local jumps in Q across the wave k.

The amplifier A_k is then simply

$$A_k = A(r_i^{(k)}) \qquad (49)$$

where A is any of the amplifying functions given by equations (44) and(45).

2.2.4 AN ALGORITHM FOR THE ONE-DIMENSIONAL CASE

Here we summarise the main steps involved in the implementation of WAF as applied to the homogeneous one-dimensional Euler equations (1).

Having specified the domain length, the number of computing cells M and the grid size Δx the following operations are performed at every time step n:

(1) Solve the Riemann problem with data (U_i, U_{i+1}) and store:

(i) the wave speeds into WS(1,i), WS(2,i), WS(3,i).

(ii) the ρ-jumps across each wave into WJ(1,i), WJ(2,i), WJ(3,i).

(iii) the star-state values p^*, u^*, ρ_L^* and ρ_R^* into SS(k,i), k=1 to 4.

Here the loop runs from i = -1 to M+1.

(2) Apply the CFL condition, based on true wave speeds given by the solution to local Riemann problems, to find Δt.

(3) For each i, i=0 to M.

(i) Compute the local Courant numbers
ν_k = WS(k,i) $\Delta t/\Delta x$, k = 1, 3.

(ii) Compute the amplifiers A_k, k = 1, 2, 3.

(iii) Modify Courant numbers $\bar{\nu}_k = A_k \nu_k$

(iv) Compute the intercell fluxes according to (46), say. Store values into FI(1, i), FI(2, i), FI(3, i).

(4) Advance to the next time level n+1 using the conservative formula (5).

3. RIEMANN SOLVERS.

In this section we present an exact Riemann solver as well as approximate Riemann solvers for use with the WAF method.

3.1 AN EFFICIENT EXACT RIEMANN SOLVER.

Recall that the ideal-gas Euler equations in differential conservation form are

$$\begin{bmatrix} \rho \\ \rho u \\ E \end{bmatrix}_t + \begin{bmatrix} \rho u \\ \rho u^2 + p \\ u(E + p) \end{bmatrix}_x = \begin{bmatrix} 0 \\ 0 \\ 0 \end{bmatrix} \qquad (1)$$

with ρ, u, p denoting density, velocity and pressure. E is total energy given by

$$E = \frac{1}{2} \rho u^2 + \rho e \qquad (2)$$

where e is the specific internal energy given by the ideal equation of state

$$e = e(\rho, p) = \frac{p}{(\gamma-1)\rho} \tag{3}$$

Equations (1) can be written as

$$U_t + F(U)_x = 0 \tag{4}$$

with the obvious meaning for the vectors of conserved variables U and the vector of fluxes F.

The Riemann problem for (4) is the initial value problem with data

$$U(0, x) = \begin{cases} U_L, & x < 0 \\ U_R, & x > 0 \end{cases} \tag{5}$$

where U_L and U_R are constant states. The solution of (4) - (5) in the x-t plane is depicted in Fig. 2. The middle wave is a contact discontinuity; the left and right waves (usually called acoustic waves) are either shock or rarefaction waves.

Both the pressure p_* and particle velocity u_* are constant in the "star" region between the acoustic waves while ρ changes discontinuously from ρ_{*L} to ρ_{*R} across the contact discontinuity. The key step in solving the complete Riemann problem is to solve for p_*. This is accomplished by deriving a single algebraic (non-linear) equation for p_*.

Following Toro (1989c) we write

$$f(p_*, U_L, U_R) \equiv f_L(p_*, U_L) + f_R(p_*, U_R) + \Delta u = 0 \tag{6}$$

with

$$\Delta u = u_R - u_L \tag{7}$$

The functions f_L and f_R are derived from relations across the acoustic waves on the left and right. They depend on (i) the unknown pressure p_* (ii) the data (U_L or U_R) and (iii) the type of the acoustic wave (either shock or rarefaction). These functions are

$$f_S = \begin{cases} \dfrac{2a_S}{(\gamma-1)}\left[H_S^{\frac{\gamma-1}{2\gamma}} - 1\right], & \text{if } p \le p_S \\ & \text{(rarefaction)} \\ (p - p_S)\left[\dfrac{A_S}{B_S + p}\right]^{1/2}, & \text{if } p > p_S \end{cases} \tag{8}$$

with S = L or R and

$$A_s = \frac{2}{(\gamma+1)\rho_s} \quad , \quad B_s = \frac{(\gamma-1)}{(\gamma+1)} p_s \quad , \quad H_s = \frac{p_*}{p_s} \tag{9}$$

The symbols a_L, a_R denote the sound speed on the left and right states respectively. As f in (6) is monotone, a unique solution for physically admissible data exists, and thus a Newton-Raphson iteration procedure for (6) to find p_* works well.

Once p_* has been found u_* follows as

$$u_* = \tfrac{1}{2}(u_L + u_R) + \tfrac{1}{2}(f_R - f_L) \tag{10}$$

The density values ρ_{*L} and ρ_{*R} either side of the contact discontinuity are

$$\rho_{*L} = \begin{cases} \rho_L H_L^{1/\gamma}, & \text{if } H_L \le 1 \text{ (rarefaction)} \\ \rho_L \left[\dfrac{(\gamma+1)H_L + \gamma - 1}{(\gamma-1)H_L + \gamma + 1} \right], & \text{if } H_L > 1 \text{ (shock)} \end{cases} \tag{11}$$

and

$$\rho_{*R} = \begin{cases} \rho_R H_R^{1/\gamma}, & \text{if } H_R \le 1 \text{ (rarefaction)} \\ \rho_R \left[\dfrac{(\gamma+1)H_R + \gamma - 1}{(\gamma-1)H_R + \gamma + 1} \right], & \text{if } H_R > 1 \text{ (shock)} \end{cases} \tag{12}$$

Now we know the complete solution for the star state (Fig. 2). When using the Riemann problem solution numerically we also need to find the wave speeds. We select

$$\left.\begin{aligned} \lambda_1 &= \begin{cases} u_L - a_L & \text{if } H_L \le 1 \\ u_L - a_L \left[1 + \dfrac{(\gamma+1)}{2\gamma}\left(H_L - 1\right) \right]^{1/2} & \text{if } H_L > 1 \end{cases} \\ \lambda_2 &= u_* \\ \lambda_3 &= \begin{cases} u_R + a_R & \text{if } H_R \le 1 \\ u_R + a_R \left[1 + \dfrac{(\gamma+1)}{2\gamma}\left(H_R - 1\right) \right]^{1/2} & \text{if } H_R > 1 \end{cases} \end{aligned}\right\} \tag{13}$$

For the case of locally sonic flow the exact solution along the t-axis is

$$\left.\begin{aligned} u &= \frac{2}{(\gamma+1)}\left[a_L + \tfrac{1}{2}(\gamma-1)u_L\right] \\ a &= a_L + \tfrac{1}{2}(\gamma-1)(u_L - u) \\ \rho &= \rho_L\left(\frac{a}{a_L}\right)^{\frac{2}{(\gamma-1)}} \\ p &= p_L\left(\frac{\rho}{\rho_L}\right)^{\gamma} \end{aligned}\right\} \qquad (14)$$

Similarly, for a right 'sonic' rarefaction we have

$$\left.\begin{aligned} u &= \frac{2}{(\gamma+1)}\left[\tfrac{1}{2}(\gamma-1)u_R - a_R\right] \\ a &= a_R + \tfrac{1}{2}(\gamma-1)(u - u_R) \\ \rho &= \rho_R\left(\frac{a}{a_R}\right)^{\frac{2}{(\gamma-1)}} \\ p &= p_R\left(\frac{\rho}{\rho_R}\right)^{\gamma} \end{aligned}\right\} \qquad (15)$$

3.2 A ROBUST APPROXIMATE RIEMANN SOLVER (RARS)

By studying in detail the behaviour of the function f(p) given by (6) we derive an approximate Riemann solver that requires no iteration. Given data ρ_L, u_L, p_L and ρ_L, u_R, p_R the function f(p) behaves as shown in Fig. 6. It is monotone and concave down as we shall demonstrate.

The first derivatives of f_S(S = L, R) with respect to p are

$$f_S' = \begin{cases} \dfrac{a_S}{\gamma p_S}\left(\dfrac{p}{p_S}\right)^{-\frac{(\gamma+1)}{2\gamma}}, & p \le p_S \\ \left(\dfrac{A_S}{B_S + p}\right)^{1/2}\left[1 - \dfrac{(p-p_S)}{2(p+B_S)}\right], & p > p_S \end{cases} \qquad (16)$$

As $f' = f_L' + f_R'$ and by inspection $f_S' > 0$ for S = L, R the function f(p) is monotone as claimed. A consequence of this is that the Newton-Raphson method to find iteratively the solution $p = p_*$ of f (p) = 0 will always converge.

The second derivatives of the functions f_S (S = L, R) are

$$f_S'' = \begin{cases} -\dfrac{(\gamma+1)a_S}{2\gamma^2 p_S^2}\left(\dfrac{p}{p_S}\right)^{-\frac{(3\gamma+1)}{2\gamma}}, & p \le p_S \\ -\dfrac{1}{4}\left(\dfrac{A_S}{B_S+p}\right)^{1/2}\left[\dfrac{4B_S+3p+p_S}{(B_S+p)^2}\right], & p > p_S \end{cases} \tag{17}$$

Since $f'' = f_L'' + f_R''$ and $f_S'' < 0$ for S = L, R the function f(p) is concave down as claimed.

From equation (16) it can be seen that $f_S' \to \infty$ as $p \to 0$ and $f_S' \to 0$ as $p \to \infty$. This behaviour of f_S and thus of f(p) has implications when searching for approximate values to the zero p_* of f(p) = 0.
The velocity difference $\Delta u = u_R - u_L$ and the pressure values p_L, p_R are the most important parameters. With reference to Fig. 6 we define

$$\left.\begin{aligned} p_m &= \min\{p_L, p_R\} \\ p_M &= \max\{p_L, p_R\} \end{aligned}\right\}$$

and note that if

$$f_m = f(p_m) \le 0 \text{ and}$$

$$f_M = f(p_M) \ge 0 \text{ then}$$

the solution p_* satisfies $p_m \le p_* \le p_M$.

For given p_L, p_R it is the velocity difference Δu which determines the value of p_*. Three intervals I_1, I_2, I_3 can be identified; these are given by

$$\left.\begin{aligned} I_1 &= (0, p_m) \\ I_2 &= [p_m, p_M] \\ I_3 &= (p_M, \infty) \end{aligned}\right\} \tag{19}$$

For sufficiently large Δu (as $(\Delta u)_3$ in Fig. 6) p_* lies in I_1 and thus $p_* < p_L$, $p_* < p_R$ and so the two acoustic waves are rarefaction waves. For Δu as $(\Delta u)_2$ in Fig. 6 p_* lies between p_L and p_R and hence one acoustic wave is a rarefaction wave and the other is a shock wave. For sufficiently small values of Δu p_* lies in I_3, that is $p_* > p_L$, $p_* > p_R$ i.e. both acoustic waves are shock waves. The interval where p_* lies can easily be identified by noting

the signs of f_m and f_M.

If f_m, $f_M > 0$ then $p_* \in I_1$ (two rarefactions). If f_m and f_M have opposite signs then p_* lies in I_2 (one shock, one rarefaction); if f_m, $f_M < 0$ then $p_* \in I_3$ (two shocks). Evaluating f_m and f_M is economical as

$$\left.\begin{aligned} f(p_L) &= f_R(p_L) + \Delta u \\ f(p_R) &= f_L(p_R) + \Delta u \end{aligned}\right\} \qquad (20)$$

A final observation on the behaviour of f(p). In I_1 both f′ and f′′(p) vary rapidly. As p increases the shape of f(p) tends to resemble that of a straight line; recall that f′ and f′′ → 0 as p → ∞.

From a precise knowledge of the properties of f(p), there are several routes to finding an approximate solution for p_*. After having tried a few possibilities we propose the following method.

(i) Compute f_m and f_M according to (20). This is like a single f(p) - function evaluation.

(ii) Identify the interval where the solution lies by using signs of f_m and f_M.

(iii) If $p_* \in I_1$ then the solution is exact and is given by

$$p_* = p_{TR} = \left[\frac{a_L + a_R + (u_L - u_R)/(\gamma-1)/2}{a_L/p_L^{\frac{\gamma-1}{2\gamma}} + a_R/p_R^{\frac{\gamma-1}{2\gamma}}} \right]^{\frac{2\gamma}{\gamma-1}}$$

(iv) If $p_* \in I_2$ or $p_* \in I_3$ perform another function evaluation; we take

$$f_{TR} = f(p_{TR})$$

(v) Fit a straight line through points (p_m, f_m) and (p_{TR}, f_{TR}) if $p_* \in I_2$ or through (p_M, f_M) and (p_{TR}, f_{TR}) if $p_* \in I_3$ to find the approximate value to p_*.

The procedure requires, effectively, two function evaluations. Note that there are three points available and a quadratic fit is tempting. The extra arithmetic involved is unattractive. Moreover, the selective linear fit procedure just described, apart from its simplicity, has an interesting property: If the states U_L and U_R are connected by a single shock, a single rarefaction or a single contact discontinuity, then the approximate solution as given by our algorithm is the exact solution. Having found p_* all other quantities follow as in section 3.1.

3.3. A LINEARISED RIEMANN SOLVER AND RIEMANN-SOLVER ADAPTATION.

By writing the Euler equations is primitive variables and performing a local linearization about a state with density $\bar{\rho}$and sound speed $\bar{a}$ one finds directly the solution for the state star (Fig. 2) as

$$\left.\begin{aligned} u_* &= \tfrac{1}{2}(u_L + u_R) - \tfrac{1}{2}(p_R - p_L)/B_1 \\ p_* &= \tfrac{1}{2}(p_L + p_R) - \tfrac{1}{2}(u_R - u_L)B_1 \\ \rho_{*_L} &= \rho_L + (u_L - u_*)B_2 \\ \rho_{*_R} &= \rho_R + (u_* - u_R)B_2 \end{aligned}\right\} \qquad (21)$$

$$B_1 = \bar{\rho}\,\bar{a}\,, \quad B_2 = \bar{\rho} \,/\, \bar{a}$$

The averaged values $\bar{\rho}$ and $\bar{a}$ can be selected in a variety of ways. Here we give

$$\bar{a} = \tfrac{1}{2}(a_L + a_R)\ ; \quad \bar{\rho} = (\rho_L \rho_R)^{1/2} \qquad (22)$$

Note that an isolated contact discontinuity is recognized exactly. For numerical purposes this is a welcome property of the linearised Riemann solver; capturing contacts is more difficult than capturing shocks. We denote the linearised approximate Riemann solver by LARS. More details are found in the paper by Toro (1991c)

We wish to use the linearised Riemann solver (21) only in regions of slowly varying data. To this end we define

$$p_m = \min\{p_L, p_R\};\ p_M = \max\{p_L, p_R\};\ Q = p_M/p_m \qquad (23)$$

and restrict the use of LARS to cases in which

$$p_m \leq p_* \leq p_M \qquad (24)$$

that is, cases in which the acoustic waves are both rarefaction waves or both shock waves are treated using the exact Riemann solver, or any other robust

Riemann solver such as the RARS or the improved HLLC solver to be discussed later. It can be shown that such restriction in pressure results in a restriction on the velocity difference Δu given as

$$-B \le \Delta u \le B \quad \text{with} \quad B = \frac{p_m(Q-1)}{B_1} \tag{25}$$

with B_1 as given in (21).

Some empiricism for switching between LARS and the exact solver is still needed when selecting the value of Q in (25). Applications suggest that Q=2 is more than adequate to reduce the use of the exact solver (expensive) to less than 1% .

Application of this linearisation to the steady, supersonic Euler equations for two and three dimensions has successfully been carried out and is to appear in a paper by Toro and Chou (1991). For this case the CPU time saving factor is three.

3.4. THE HARTEN-LAX-VAN LEER RIEMANN SOLVER (HLL)

A very simple type of approximations to the solution of the Riemann problem was proposed by Harten, Lax and van Leer (1983). Their basic assumption is that the only waves present are the left and right acoustic waves. If estimates λ_1 and λ_3 for the lower and upper limits of the speeds of these acoustic waves are available then one can easily solve for the conserved variables and fluxes in the "star" region between the acoustic waves.

Consider Fig. 7. Evaluation of the integral form of the conservation laws (4) in the rectangle ABCD gives

$$U^*_{i+1/2} = \frac{\lambda_3 U_R - \lambda_1 U_L - (F_R - F_L)}{\lambda_3 - \lambda_1} \tag{26}$$

where $U^*_{i+1/2}$ is the vector of conserved variables between the acoustic waves. These values can be used directly to either compute fluxes between the acoustic waves, if version (12) (section 2) of WAF is to be used, or they can be used to compute a weighted average state, if version (14) (section 2) of WAF is to be used. For the former version of WAF, one can also compute a "star" flux directly as

$$F^{*}_{i+1/2} = \frac{\lambda_3 F_L - \lambda_1 F_R + \lambda_1 \lambda_2 (U_R - U_L)}{\lambda_3 - \lambda_1} \qquad (27)$$

Expressions (26) and (27) are only valid for the case of Fig.7, i.e. $\lambda_1 < 0$ and $\lambda_3 > 0$.

This approximate Riemann solver has one intermediate "star" state only. That is to say, the density (temperature or internal energy) is assumed constant across the contact discontinuity. As a consequence, contact discontinuities are badly smeared.

The major problem with this Riemann solver is to find reliable and sufficiently simple estimates λ_1 and λ_3 for the lower and upper bounds for the wave speeds. Davis (1988) proposed a number of procedures for these wave-speed estimates. There is scope for the imagination in choosing the wave estimates. An important consideration in doing so is the entropy condition (see Harten (1983) and Harten et. al. (1983) for details).

A possible choice for λ_1 and λ_3 in (26) - (27) is the wave speeds given by the Roe approximation,provided the entropy fix has been incorporated into the Roe scheme. Davis made the interesting observation that the choice

$$\lambda_3 = \Delta x/\Delta t \ , \ \lambda_1 = -\lambda_3 \qquad (28)$$

gives a flux $F^{*}_{i+1/2}$ associated with the Lax-Friedrich's scheme. Other obvious choices reproduce "star" fluxes $F^{*}_{i+1/2}$ associated with familiar schemes (e.g. Rusanov's method).

Here we present another way of choosing estimates λ_1 and λ_3 for the wave speeds. Consider the isentropic equations of Gas Dynamics. This is a 2 x 2 system of hyperbolic equations with eigenvalues (wave speeds) $\lambda_1 = u-a$ and $\lambda_3 = u+a$. Assume that the two waves in the Riemann problem for the isentropic equations are rarefaction waves. Then we can find approximate solutions for the speed u^{*} and the sound speed a^{*} between the acoustic waves. These are

$$
\begin{aligned}
u^* &= \tfrac{1}{2}(u_L + u_R) + (a_L - a_R)/(\gamma-1) \\
a^* &= \tfrac{1}{2}(a_L + a_R) + (\gamma-1)(u_L - u_R)/4
\end{aligned}
\tag{29}
$$

Then choose

$$
\begin{aligned}
\lambda_1 &= \min\left\{u_L - a_L,\ u^* - a^*\right\} \\
\lambda_3 &= \max\left\{u_R + a_R,\ u^* + a^*\right\}
\end{aligned}
\tag{30}
$$

Application of WAF with the HLL Riemann solver using the wave speeds (29)-(30) gives very satisfactory results. It is worth remarking that for rarefaction waves the estimates are always correct, but for shocks they may fail to bound the shock speed. A possible improvement is as follows.

Using estimates (29)-(30) and the integral form of the Euler equations (1) on the rectangle ABCD of Fig. 7 one obtains eqn.(26) for the conserved variables $(\rho,\ \rho u,\ E)^T$ between the acoustic waves. Denoting the right-hand side of (26) by R one has the vector equation

$$
(\rho^*, \rho^* u^*, E^*)^T = (R_1, R_2, R_3)^T \tag{31}
$$

Hence

$$
\left.
\begin{aligned}
\rho^* &= R_1 \\
u^* &= R_2/R_1 \\
p^* &= (\gamma-1)(R_3 - \tfrac{1}{2}R_2^2/R_1)
\end{aligned}
\right\}
\tag{32}
$$

A new sound speed $a^* = (\gamma p^*/\rho^*)^{1/2}$ can now be computed from (32). Then we set λ_1 and λ_3 as in (30) but with revised values for u^* and a^* given by (32).

The resulting scheme (30) for choosing the wave speeds together with the modification (32) gives a very simple version of the HLL Riemann solver. Extensive numerical experiments carried out by the author (unpublished) also show that the resulting numerical methods are very robust.

3.5. AN IMPROVED VERSION OF THE HLL RIEMANN SOLVER (HLLC).

The HLL Riemann solver, particularly with the proposed modification performs very well indeed for 2 x 2 hyperbolic systems (e.g. shallow water equations or isentropic gas dynamics). For larger systems however, such as the Euler equations, contact discontinuities or shear waves are ruined. One can remedy this anomaly of the HLL solver by restoring the wave associated with the contact discontinuity as advanced in the paper by Toro (1991b).

Assume a wave configuration as in Fig. 8. Suppose we use the estimates (30) derived from equations (32). Now we have an estimate for the wave speed of the contact discontinuity, $\lambda_2 = u^*$. The integral form of the Euler equations (see eq. 4, section 2), when evaluated on ABEF of Fig. 8 give

$$F_L^* = F_L + \lambda_1(U_L^* - U_L) \tag{33}$$

Integration on BCDE gives

$$F_R^* = F_R + \lambda_3(U_R^* - U_R) \tag{34}$$

The vector equation (33) can be re-written as

$$\lambda_1 U_L^* - F_L^* = S \tag{35}$$

while equation (34) can be re-arranged as

$$\lambda_3 U_R^* - F_R^* = Q \tag{36}$$

with the obvious notation for the known vectors S and Q on the right hand sides of (35) and (36). Since $\lambda_2 = u^*$ is known equations (35) give

$$\rho_L^* = S_1/(\lambda_1 - \lambda_2);\ p^* = \lambda_2 S_1 - S_2\ ;\ E_L^* = (S_3 + \lambda_2 p^*)/(\lambda_1 - \lambda_2) \tag{37}$$

From (37) the vector $U_L^* = (\rho_L^*, \rho_L^* u^*, E_L^*)$ of conserved variables is known and so the intercell flux F_L^* in (33) is now determined.

In an entirely analogous way U_R^* in equations (34) can be found. This follows from the solution

$$\rho_R^* = Q_1/(\lambda_3 - \lambda_2);\ p^* = \lambda_2 Q_1 - Q_2\ ;\ E_R^* = (Q_3 + \lambda_2 p^*)/(\lambda_3 - \lambda_2) \qquad (38)$$

Then the flux F_R^* in (34) is determined and so the WAF method can now be applied. Numerical results show that this improved version HLLC of the Harten-Lax-van Leer Riemann solver produces results of the same quality as those obtained from using the exact Riemann solver.

It should be remarked that results (33) to (38) are also valid for wave configurations other than that showed in Fig. 8. Also, for the solution for the pressure p* we in practice take a mean value from solutions (37) and (38).

4. NUMERICAL RESULTS.

Here we present some numerical results for fout test problems. Test problems 1 and 2 are one-dimensional while tests 3 and 4 are two-dimensional.

TEST 1 : SOD'S SHOCK-TUBE PROBLEM.

This problem simulates the flow in a shock tube of unit lenght with a diaphragm at x = 1/2 separating a left (L) and right (R) states given by

$$\rho_L = 1.0 \qquad \rho_R = 0.125$$
$$u_L = 0.0 \qquad u_R = 0.0$$
$$p_L = 1.0 \qquad p_R = 0.1 \qquad \gamma = 1.4$$

Results are presented in Figs. 9 to 13. The numerical solution in all cases was obtained using M = 100 cells and a CFL coefficient of 0.8. Results are displayed at time t = 0.25 units; the numerical solution is shown in symbols while the exact solution is shown by a full line. All the WAF numerical results shown in this section were obtained using the TVD function SUPERA.

Fig. 9 shows the numerical solution obtained by using the WAF method with the

exact Riemann solver and the amplifier SUPERA. The quantities shown are the density, pressure, particle velocity and specific internal energy. The smooth part of the flow is very accurately resolved, including the head and tail of the left-running rarefaction. The right-travelling shock wave is resolved with two interior points. This is comparable to the resolution of other RP methods such as Roe's second order method. The contact discontinuity is resolved with three interior points, which is satisfactory. Contacts, due to their linear character, are more difficult to resolve sharply than shock waves.

Fig. 10 shows the results obtained when using the Godunov's method, which is only first-order accurate. The smooth parts of the solution are, as expected from a first-order method, not accurately represented. The shock wave is quite sharply resolved with about five interior points but the contact discontinuity is ruined, it has eighteen interior points. Compare Fig 9 to Fig. 10. Such comparison is justified for two reasons. First, it illustrates the accuracy of the WAF method and second, the WAF method utilises exactly the same Riemann problem as the Godunov's method and yet it gives much better results.

Fig. 11 shows the results obtained by the WAF method together with the linearised Riemann solver (LARS). Note that the quality of the solution is comparable to that obtained by using the exact Riemann solver (see Fig. 9), althought for this test problem the initial pressure ratio is 10. In the adaptation procedure we use LARS for local Riemann problems with pressure ratios less than 2, which is a very conservative criterion.

Fig. 12 shows the results obtained when using the WAF method in conjunction with the Harten-Lax-van Leer, or HLL, approximate Riemann solver The two-rarefaction approximation applied to the isentropic equations is used to obtain the wave speed estimates required by the HLL solver. The resolution of the rarefaction and shock is good but that of the contact discontinuity is very poor, just as in first order methods.

Fig. 13 show the corresponding result for HLLC solver, our improved version of the Harten-Lax-van Leer, or HLL, Riemann solver. Note the improvement in the resolution of the contact discontinuity. HLLC gives results of comparable accuracy to the exact Riemann solver and yet it is significantly simpler.Current work is concerned with the extension of HLLC to gases with

general equation of state. Preliminary results for co-volume gases are very satisfactory. It is for gases with general equation of state when the efficiency of Riemann solvers (without compromising robustness) is put to the test.

TEST 2: A BLAST-WAVE PROBLEM.

This problem was proposed by Woodward and Colella (1984). The initial data consists of three constant states in a tube of unit length separated by two diaphragms place at 0.1 and 0.9. The density is everywhere unity and the velocity is zero. The pressure has the values 1000.0, 0.01 and 100.0 in the left, middle and right regions respectively; γ=1.4. Results are shown at time t = 0.028, shortly after the collision of the two leading shocks emanating from the initial discontinuities; we use 3000 cells. Fig. 14 shows the result obtained by the WAF method using the exact Riemann solver, while Fig. 15 shows WAF using the exact and the linearised (LARS) Riemann solvers adaptively. Results are virtually identical but the adaptive method gives a CPU time saving factor of 2. Fig. 16 shows the corresponding result when HLLC is used. Note the resolution of the contact discontinuity is as good as that of the exact Riemann solver. We are confident that this improved version of the Harten-Lax-van Leer Riemann solver can now be used for practical applications. Current work involves the application of HLLC to real gases.

TEST 3: A CYLINDRICAL EXPLOSION

In this two-dimensional test problem we solve the time-dependent two-dimensional Euler equations on the domain [0,2] x [0,2] in the x-y plane. The initial conditions for ρ and p are those of of TEST 1 and u = v = 0.0; the region of high pressure and high density is the circle of radius 0.35 centred at (1,1). Cells covered partially by both sets of data are re-initialised in area-weighted fashion. The solution of the problem consists of three waves, namely an outward travelling shock followed by a contact discontinuity and rarefaction wave travelling toward the centre. Both the shock and the contact will attenuate at time evolves and the mechanism that allows this is the presence of rarefaction waves following both the contact and the shock and so the post-shock and post-contact states are not horizontal as in the one-dimensional case. Fig. 17 shows the pressure distribution at time 0.3

units and Fig. 18 shows the density distribution at the same time. The expected symmetry of the circular waves is very well represented in the numerical solution. Also both the shock and the contact are sharply resolved. Along radial distance the problem is one-dimensional with geometric source terms. Fig. 19 shows a comparison between the numerical solution of the one dimensional problem obtained by using the Random Choice Method (RCM) and the WAF two-dimensional solution along one radial line. The quantities shown are density and radial velocity. For the WAF solution we have used 50 cells only while for RCM we have used 500. Good agreement is observed.

TEST 4: A MACH REFLECTION PROBLEM

This two-dimensional test problem consists of Mach 5.5 flow over a 30 degree wedge. Fig. 20 shows contours of density for the numerical solution obtained by the WAF method with Riemann solver adaptation (exact Riemann solver and LARS). Fig. 21 shows the corresponding solution using the exact Riemann solver throughout.

5. CONCLUSIONS.

The WAF numerical method as applied to the time-dependent Euler equations along with a range of Riemann solvers have been presented. Also, a Riemann-solver adaptation procedure has been proposed and tested. Numerical results for one and two-dimensional test problems show that the resulting algorithms are very satisfactory.

REFERENCES

1. Davis, S.F. 1988.
Simplified second-order Godunov-type Methods. SIAM J. Sci. and Stat. Comput., Vol. 9, No.3, pp 445 - 473.

2. Godunov, S.K. 1959
A finite difference method for the numerical computation of discontinuous solutions of the equations of fluid dynamics. Mat. Sb. 47, pp 357-393.

3. Harten, A. 1983.
High resolution schemes for hyperbolic conservation laws. J. Comput. Physics, 49 pp 357 - 393.

4. Harten, A., Lax, P.D. and van Leer, B. 1983.
On upstream differencing and Godunov-type schemes for hyperbolic conservation laws, SIAM Review 25, pp 35 - 61.

5. Osher, S 1984.
Riemann solvers, the entropy condition and difference approximations.
SIAM J. Numerical Analysis, 21, 217-235.

6. Roe, P.L. 1981.
Approximate Riemann solvers, parameter vectors, and difference schemes. J. Comput. Physics. 43: 357 - 372.

7. Toro, E.F. 1989.a.
A weighted average flux method for hyperbolic conservation laws. Proc. Royal Soc. London. A423, 401-418.

8 Toro, E.F. 1989. b.
Riemann-problem based methods for computing reactive two-phase flows.
Lecture Notes in Physics, 351 pp 472-481: Numerical Combustion. Proceedings, Juan Les Pins, Antibes, France 1989. Dervieux and Larrouturou (Eds.).

9. Toro, E.F. 1989.c.
A fast Riemann solver with constant covolume applied to the Random Choice Method. Int. J. Numer. Methods in Fluids, Vol.9, pp 1145-1164.

10. Toro, E.F. 1989.d.
TVD regions for the weighted average flux (WAF) method as applied to a model hyperbolic conservation law. Cranfield Report No.8907, June 1989. College of Aeronautics, Cranfield Institute of Technology.

11. Toro, E F 1991a
Riemann problems and the WAF method for solving the two-dimensional shallow water equations. Phil. Trans. Royal Soc. London (to appear).

12. Toro, E F 1991b

The Weighted Average Flux Method Aplied to the Euler Equations. Phil. Trans. Roy. Soc. London (submitted)

13. Toro, E F 1991c

A linearised Riemann solver for the time-dependent Euler equations of Gas Dynamics. Proc. Roy. Soc. London (to appear in September 1991).

14. Toro, E F and Chou, C. 1991

A linearised Riemann solver for the two and three-dimensional steady supersonic Euler equations. In preparation.

19. van Leer, B. 1979.

Towards the ultimate conservative difference scheme. V. A second-order sequel to Godunov's method. J. Comptational Phys. 32, 101-136.

20. Woodward P. abd Colella P. 1984

The numerical simulation of two-dimensional fluid flow with strong waves.J. Comput. Phys. 54, pp 115-173.

LEGEND TO FIGURES

Fig. 1. Control volume of dimensions Δx_i by Δt is computational cell i. New value U_i^{n+1} is given in terms of old value U_i^n and intercell fluxes.

Fig. 2. Solution of the Riemann problem with data U_L and U_R in the x-t plane. The three waves present define four piece-wise constant states. Solution is found in terms of the star region between acoustic waves.

Fig. 3. Evaluation of the intercell numerical flux for the WAF method. The simplified wave structure in the solution of the Riemann problem gives four regions k of non-dimensional lenght W_k.

Fig. 4. Ilustration of the WAF intercell flux for the linear advection equation.

Fig . 5. TVD regions in the r-A plane for WAF method as applied to the linear advection equation.

Fig. 6 Illustration of the behaviour of the function f(p) for the exact Riemann solver.

Fig. 7. Simplified wave structure for the HLL approximate Riemann solver.

Fig. 8. Wave configuration for the modified HLLC Riemann solver with restored contact wave.

Fig. 9. Comparison between the numerical (symbol) and exact (line) solutions for Test 1. The numerical results correspond to using WAF with the exact Riemann solver.

Fig. 10. Comparison between the numerical (symbol) and exact (line) solutions for Test 1. The numerical results correspond to using Godunov's method with the exact Riemann solver.

Fig. 11. Comparison between the numerical (symbol) and exact (line) solutions for Test 1. The numerical results correspond to using the WAF method with the linearised Riemann solver LARS.

Fig. 12. Comparison between the numerical (symbol) and exact (line) solutions for Test 1. WAF with the HLL and the isentropic-wave speed estimates is used.

Fig. 13. Comparison between the numerical (symbol) and exact (line) solutions for Test 1. WAF with the HLLC Riemann solver is used.

Fig. 14. WAF numerical solution to test 2 at time 0.028. Exact Riemann solver is used.

Fig. 15. Numerical solution to test 2 obtained by WAF with Riemann solver adaptation.

Fig. 16. Numerical solution to test 2 obtained by the WAF method with our

improved version HLLC of the HLL approximate Riemann solver.

Fig. 17. Computed pressure distribution for Test 3 using the WAF method with the exact Riemann solver.

Fig. 18. Computed density distribution for Test 3.

Fig. 19. Comparison of numerical results for Test 3 between the two-dimensional WAF solution (symbol) and the one-dimensional Random Choice solution (full line). WAF uses 50 cells and RCM 500.

Fig. 20. Density contours for test 4; WAF with Riemann solver adaptation is used.

Fig. 21. Density contours for test 4; WAF with the exact Riemann solver is used.

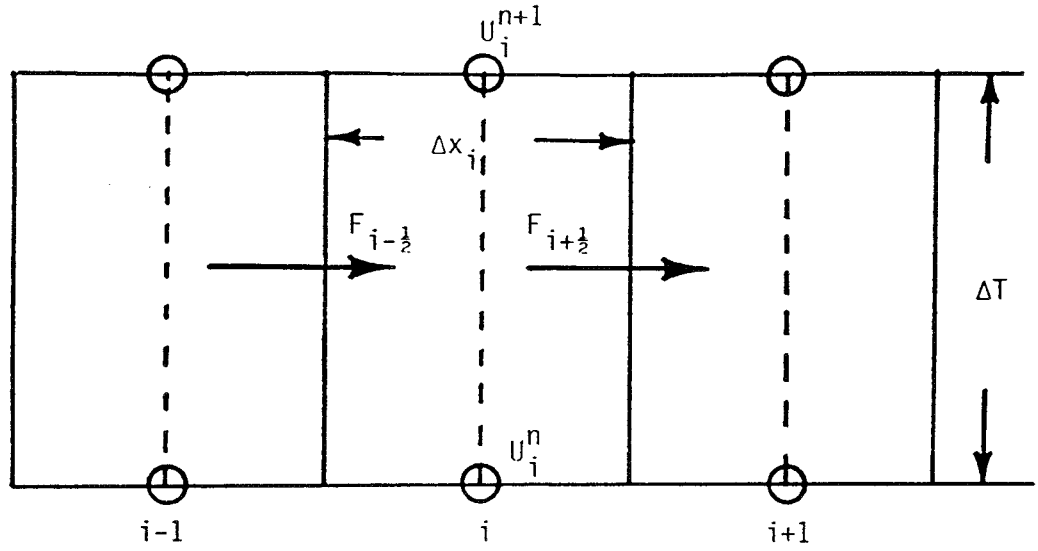

Fig.1: Control volume of dimensions Δx_i by ΔT is computational cell i. New value U_i^{n+1} is given in terms of old value U_i^n and the intercell fluxes $F_{i-\frac{1}{2}}$ and $F_{i+\frac{1}{2}}$.

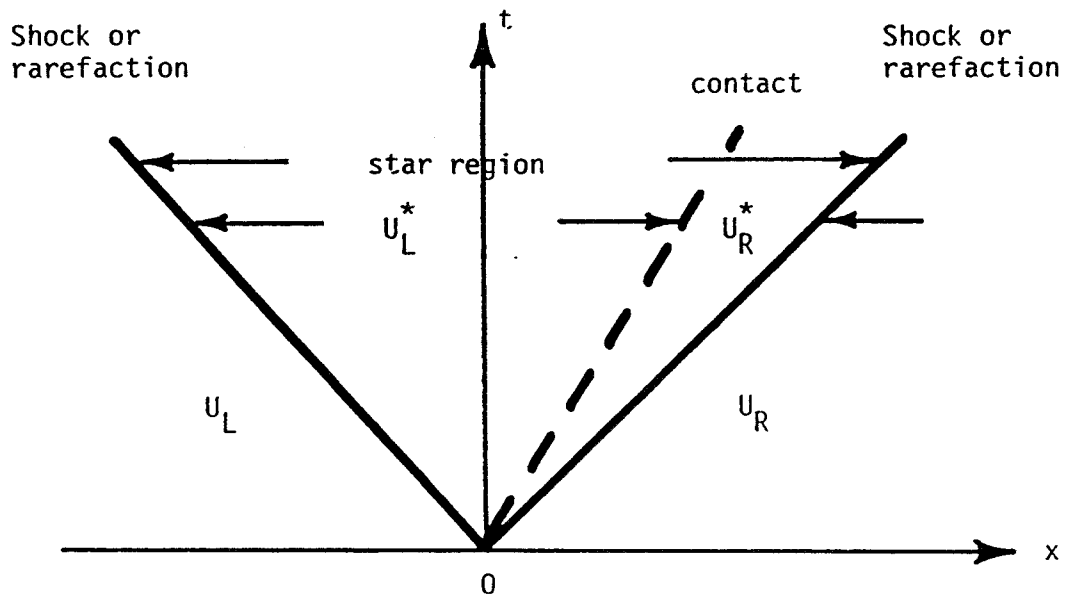

Fig.2: Solution of the Riemann problem with data $U_i(=U_L)$ and $U_{i+1}(=U_R)$ in the x - t plane.

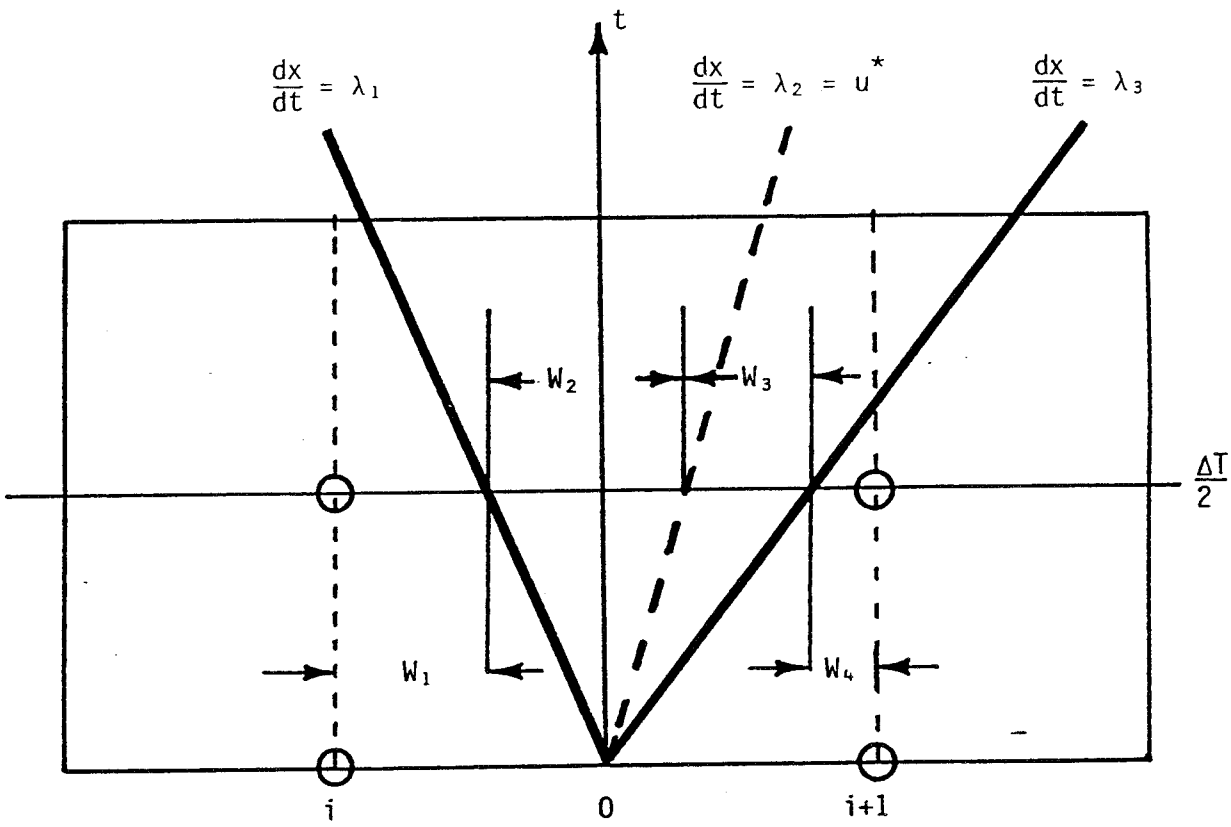

Fig.3: Evaluation of the intercell flux $F_{i+\frac{1}{2}}$ for the WAF method. The simplified wave structure gives four constant states of lengths W_1, W_2, W_3 and W_4.

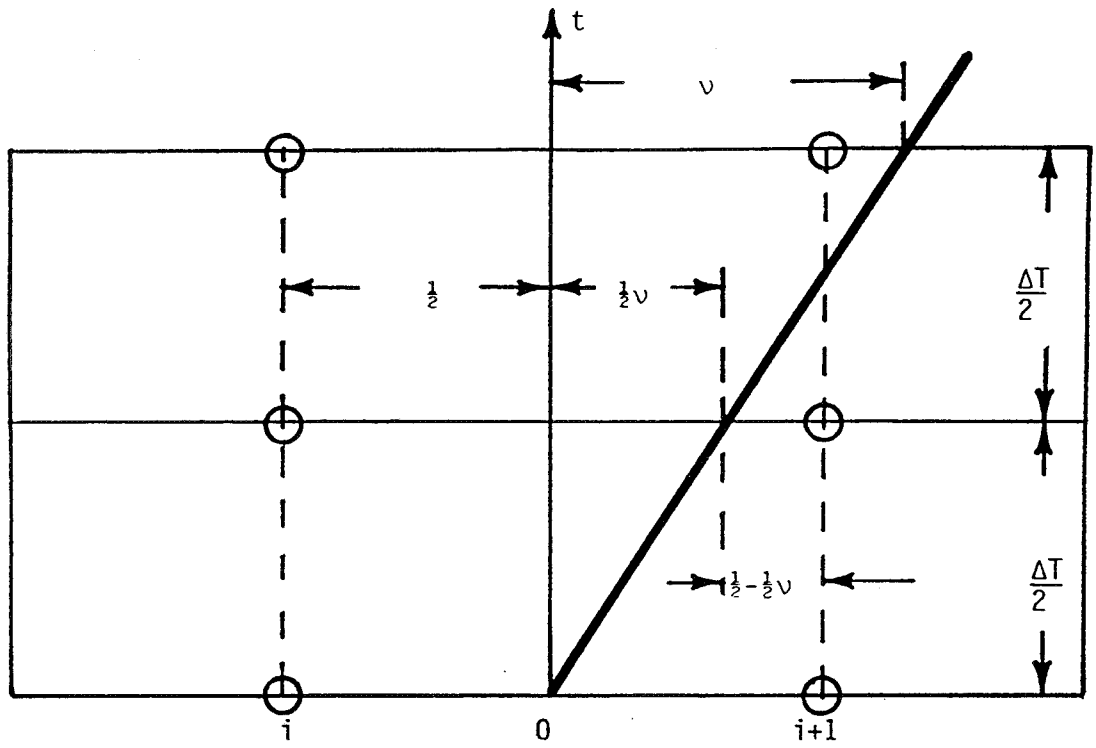

Fig. 4 Illustration of the WAF intercell flux for the model equation $u_t + au_x = 0$, $a > 0$. Cell lengths are normalised.

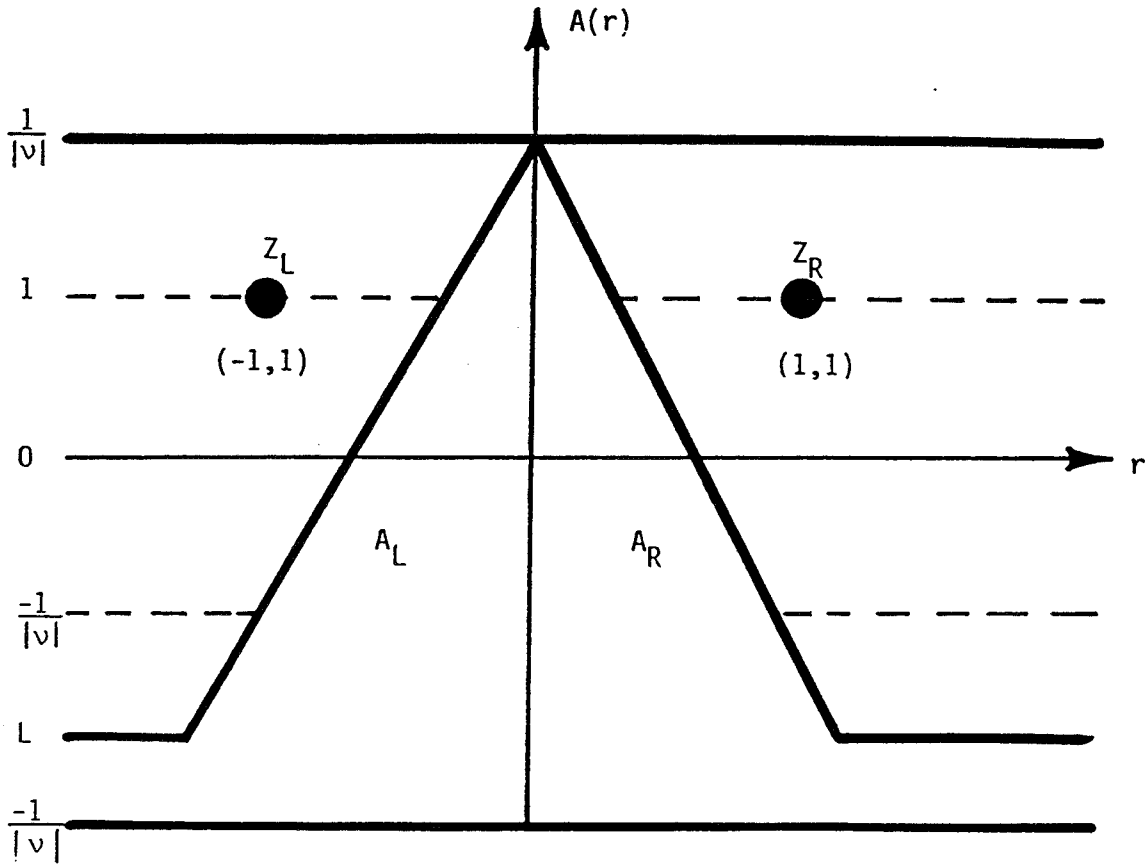

Fig. 5 TVD regions Z_L and Z_R in the r - A plane for the WAF Method as applied to the model equation.

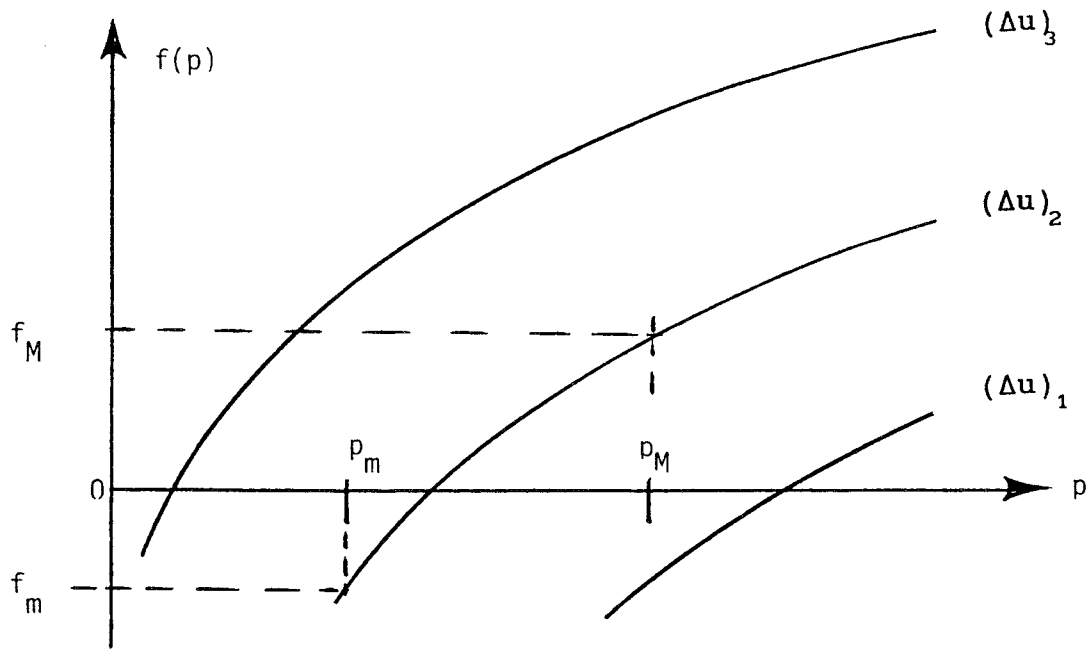

Fig. Behaviour of the exact function for pressure.

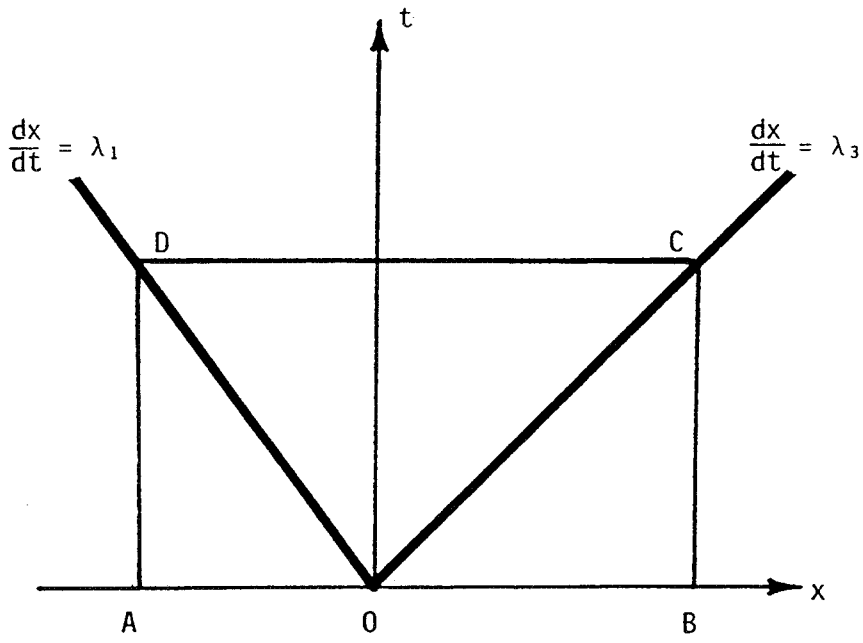

Fig. 7 Simplified wave structure for the HLL approximate Riemann solver.

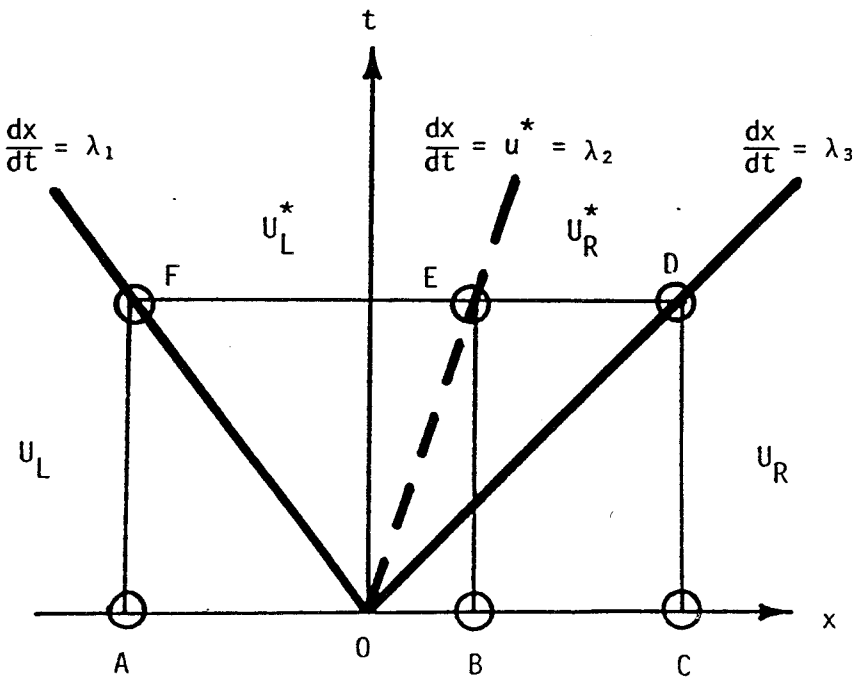

Fig. 8 Wave configuration for the modified HLL Riemann solver.

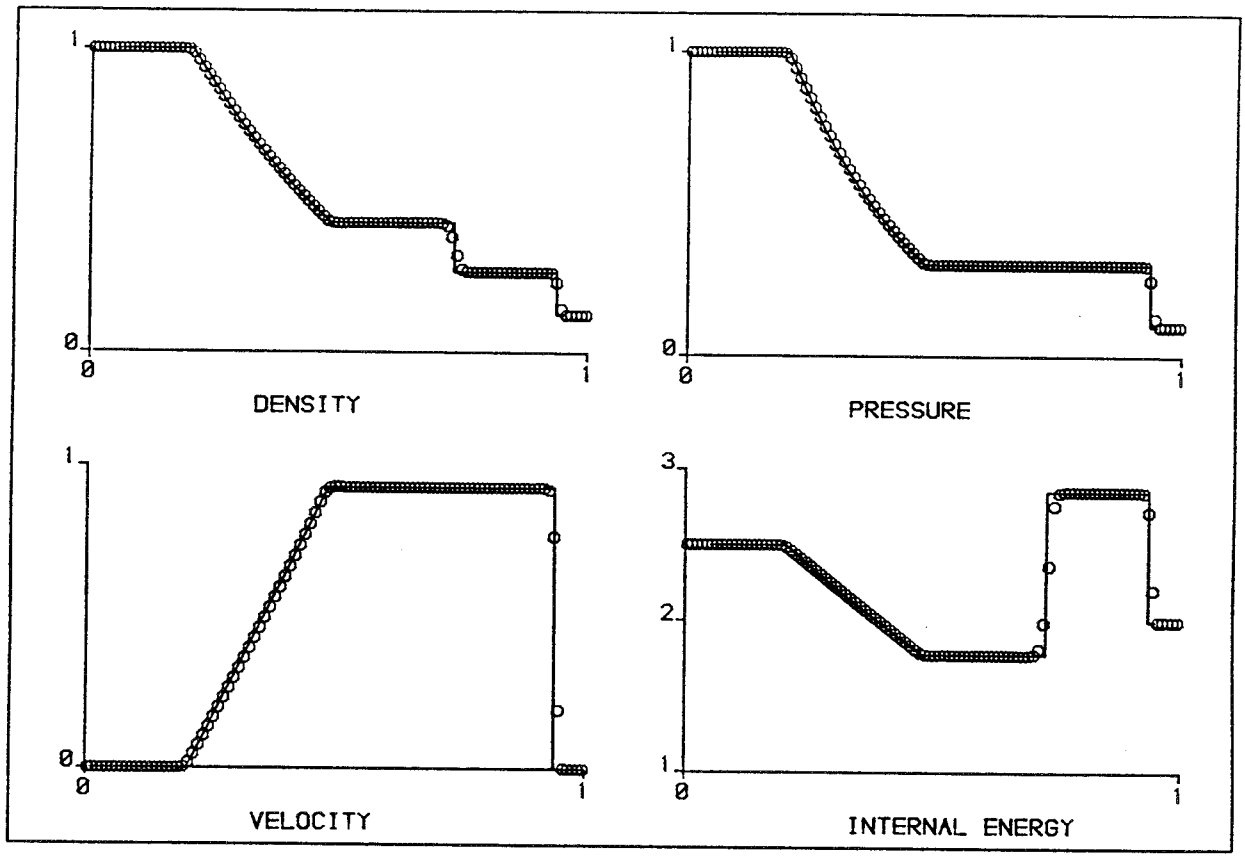
1
0
0
1
DENSITY
1
0
0
1
PRESSURE
1
0
0
1
VELOCITY
3
2
1
0
1
INTERNAL ENERGY

FIGURE

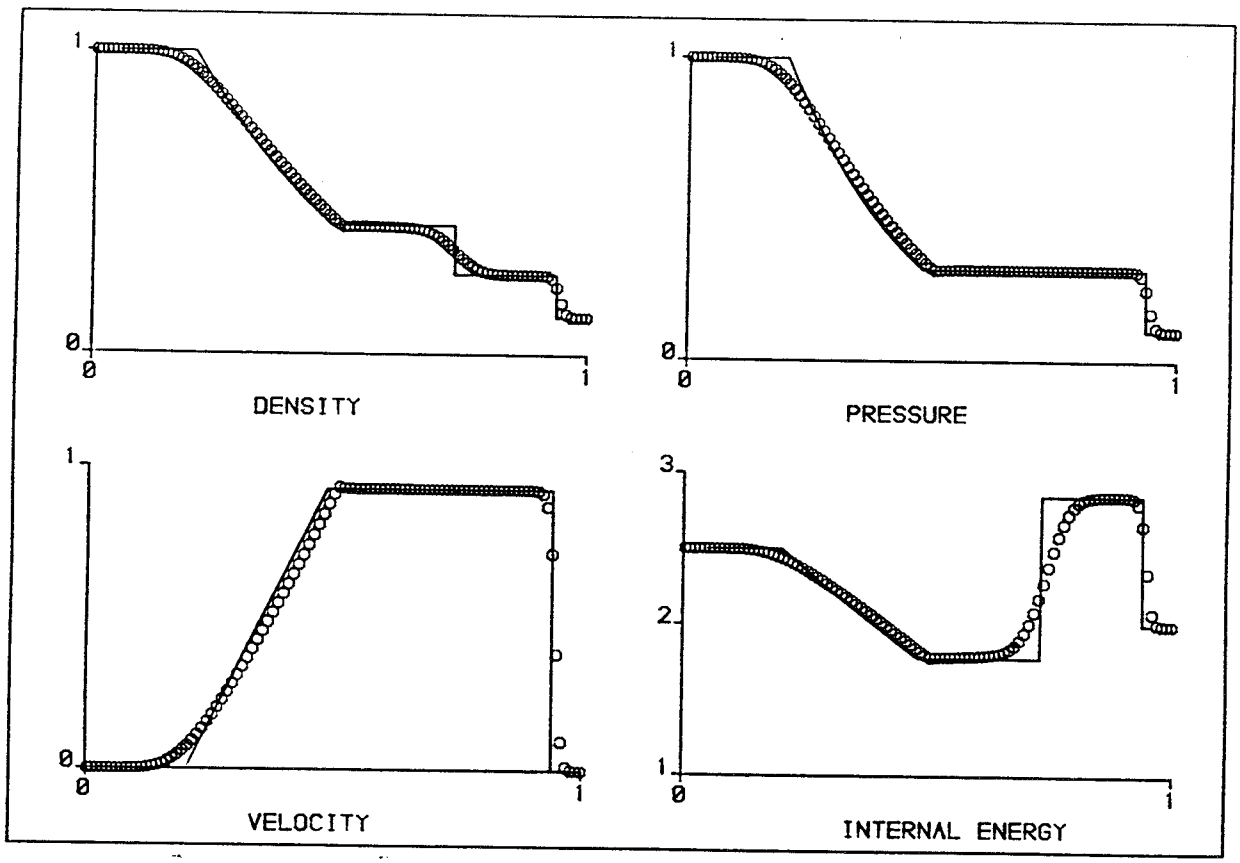
1
0
0
1
DENSITY
1
0
0
1
PRESSURE
1
0
0
1
VELOCITY
3
2
1
0
1
INTERNAL ENERGY

FIGURE 10

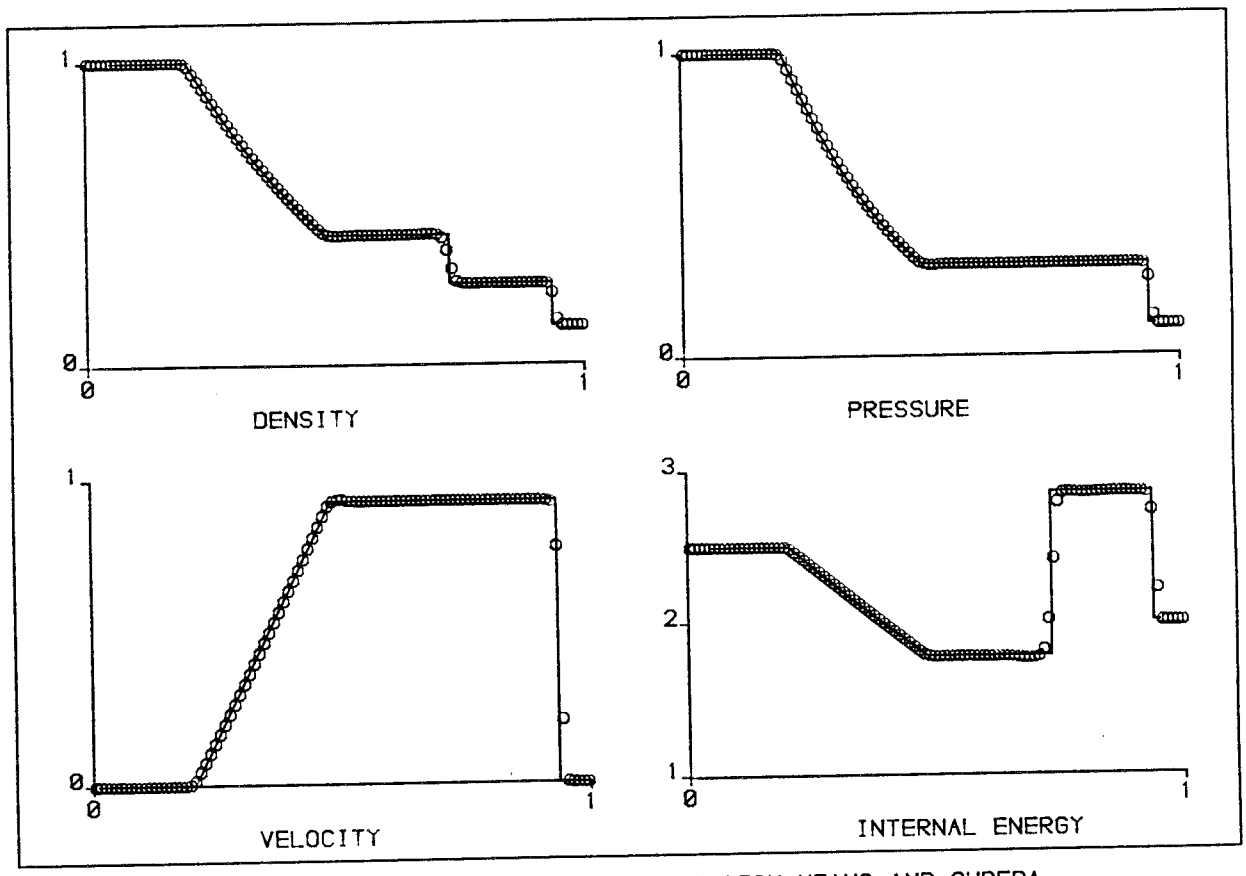

FIGURE : WAFLIN METHOD WITH ARITH AND GEOM MEANS AND SUPERA.

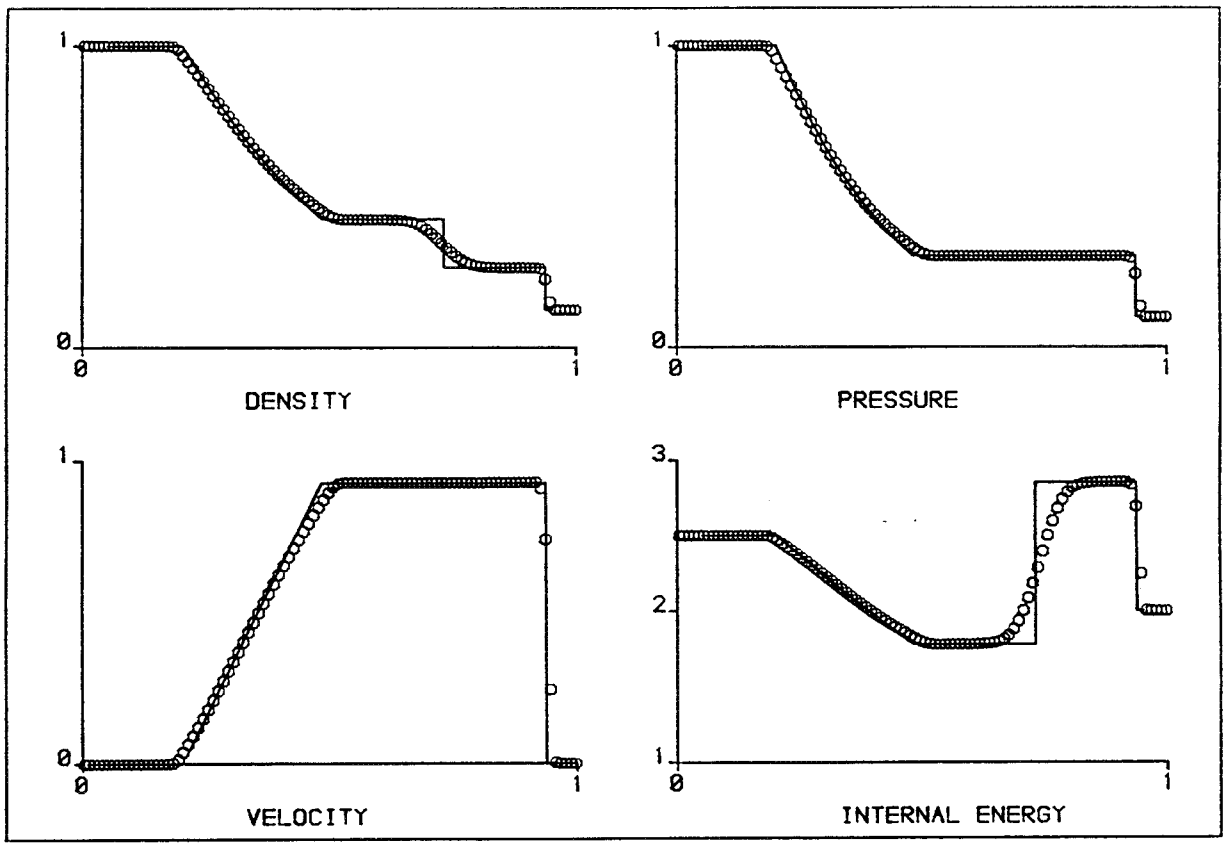
1
0
0
1
DENSITY
1
0
0
1
PRESSURE
1
0
0
1
VELOCITY
3
2
1
0
1
INTERNAL ENERGY

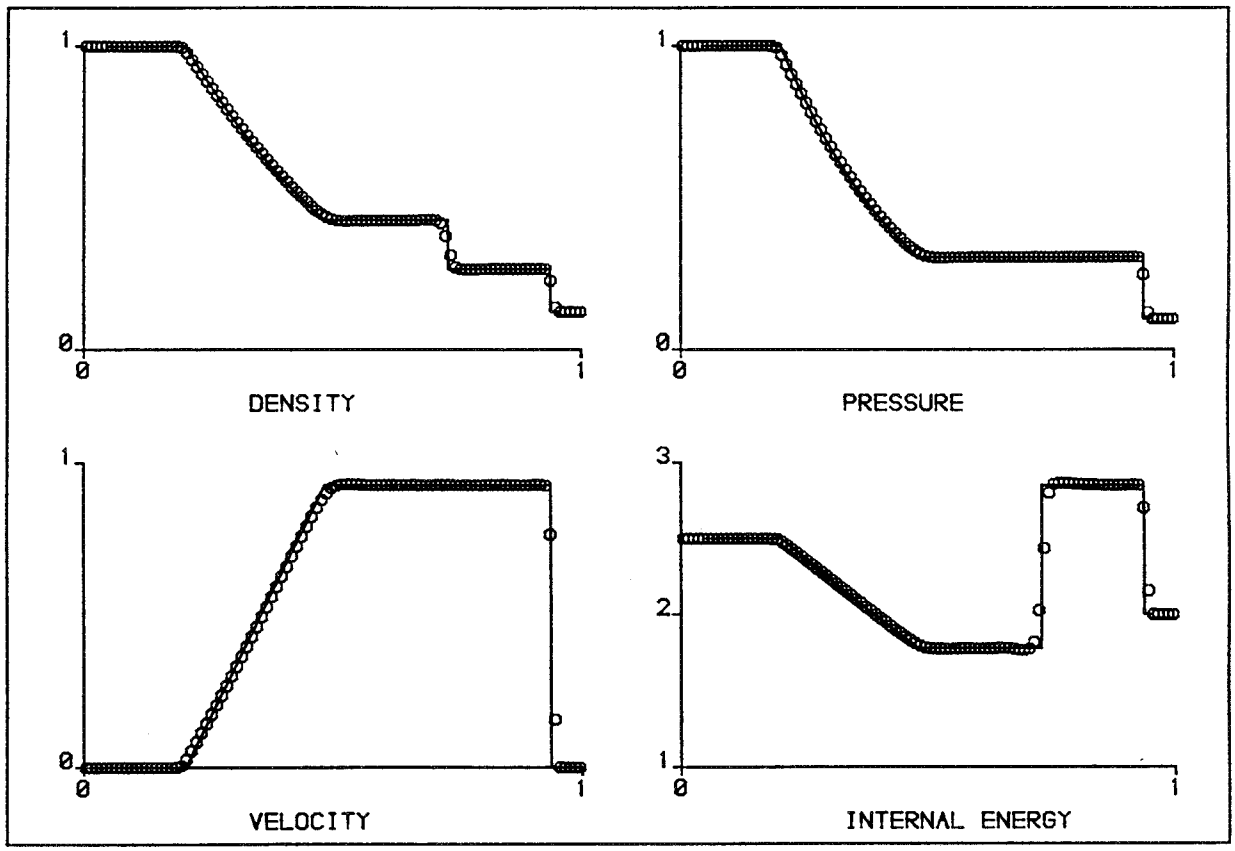

FIGURE : WAF WITH HLLC AND SUPERA

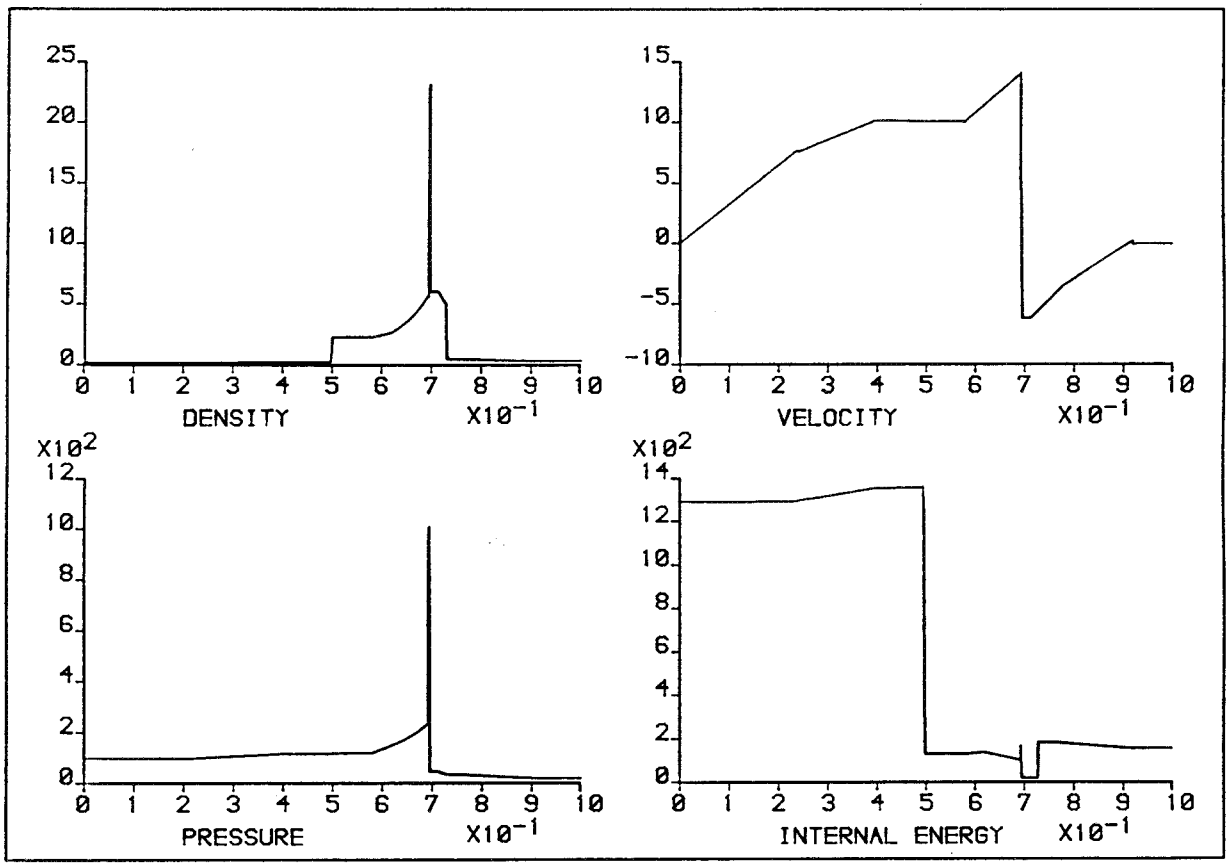
25
20
15
10
5
0
0 1 2 3 4 5 6 7 8 9 10
DENSITY
X10⁻¹
15
10
5
0
-5
-10
0 1 2 3 4 5 6 7 8 9 10
VELOCITY
X10⁻¹
X10²
12
10
8
6
4
2
0
0 1 2 3 4 5 6 7 8 9 10
PRESSURE
X10⁻¹
X10²
14
12
10
8
6
4
2
0
0 1 2 3 4 5 6 7 8 9 10
INTERNAL ENERGY
X10⁻¹

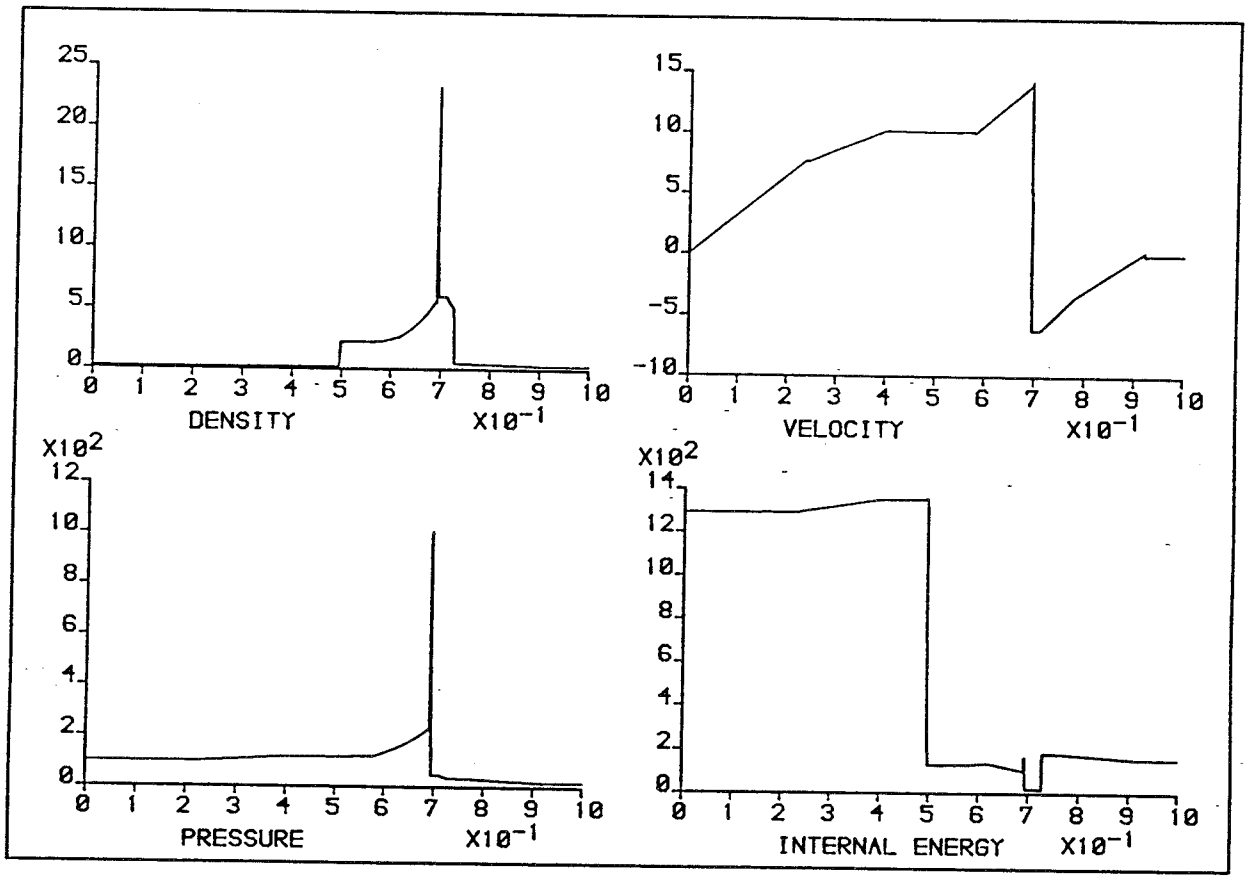
25
20
15
10
5
0
0 1 2 3 4 5 6 7 8 9 10
DENSITY
X10-1
15
10
5
0
-5
-10
0 1 2 3 4 5 6 7 8 9 10
VELOCITY
X10-1
X10²
12
10
8
6
4
2
0
0 1 2 3 4 5 6 7 8 9 10
PRESSURE
X10-1
X10²
14
12
10
8
6
4
2
0
0 1 2 3 4 5 6 7 8 9 10
INTERNAL ENERGY
X10-1

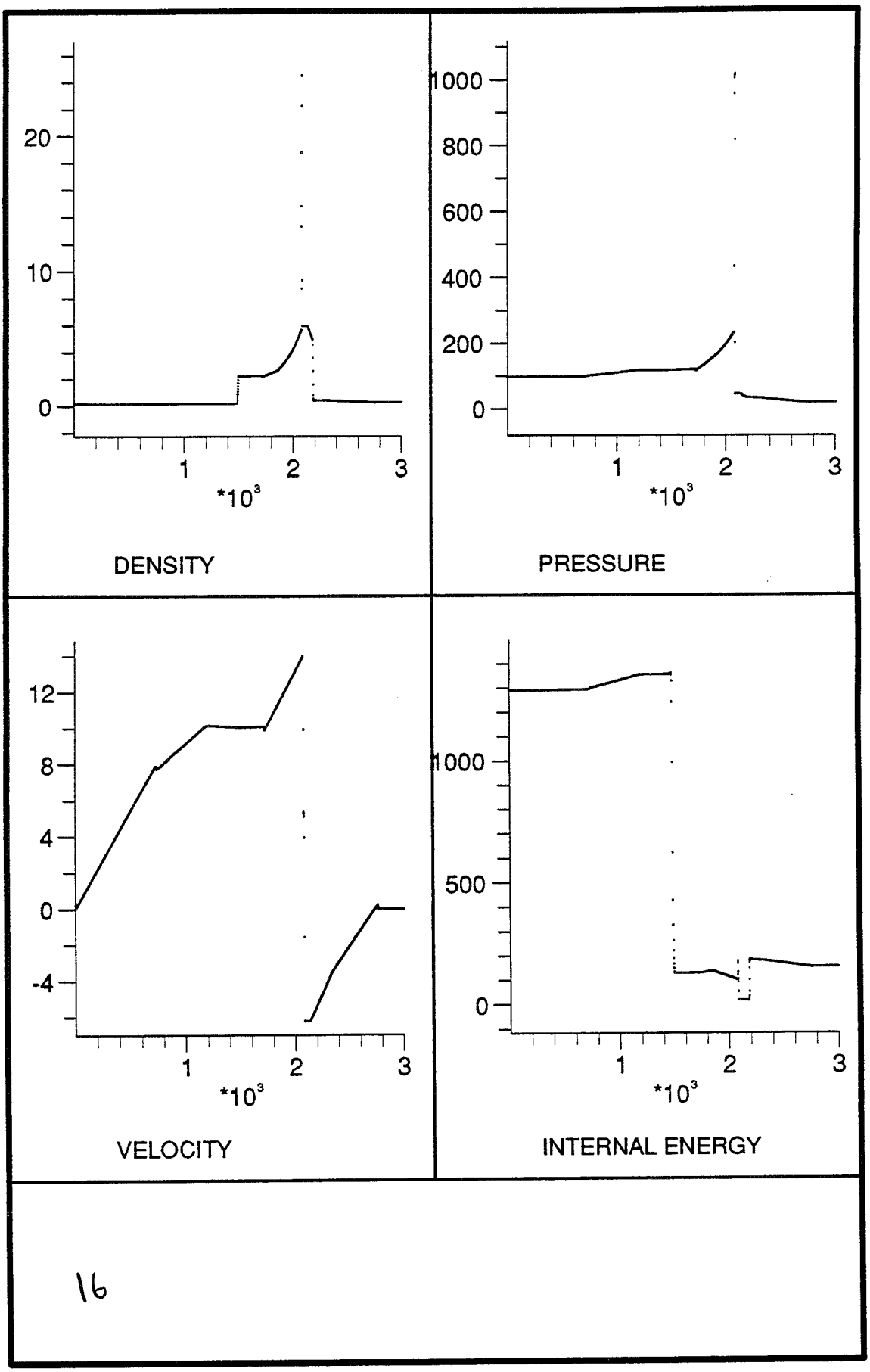
20
10
0
1
2
3
*10³
DENSITY
1000
800
600
400
200
0
1
2
3
*10³
PRESSURE
12
8
4
0
-4
1
2
3
*10³
VELOCITY
1000
500
0
1
2
3
*10³
INTERNAL ENERGY

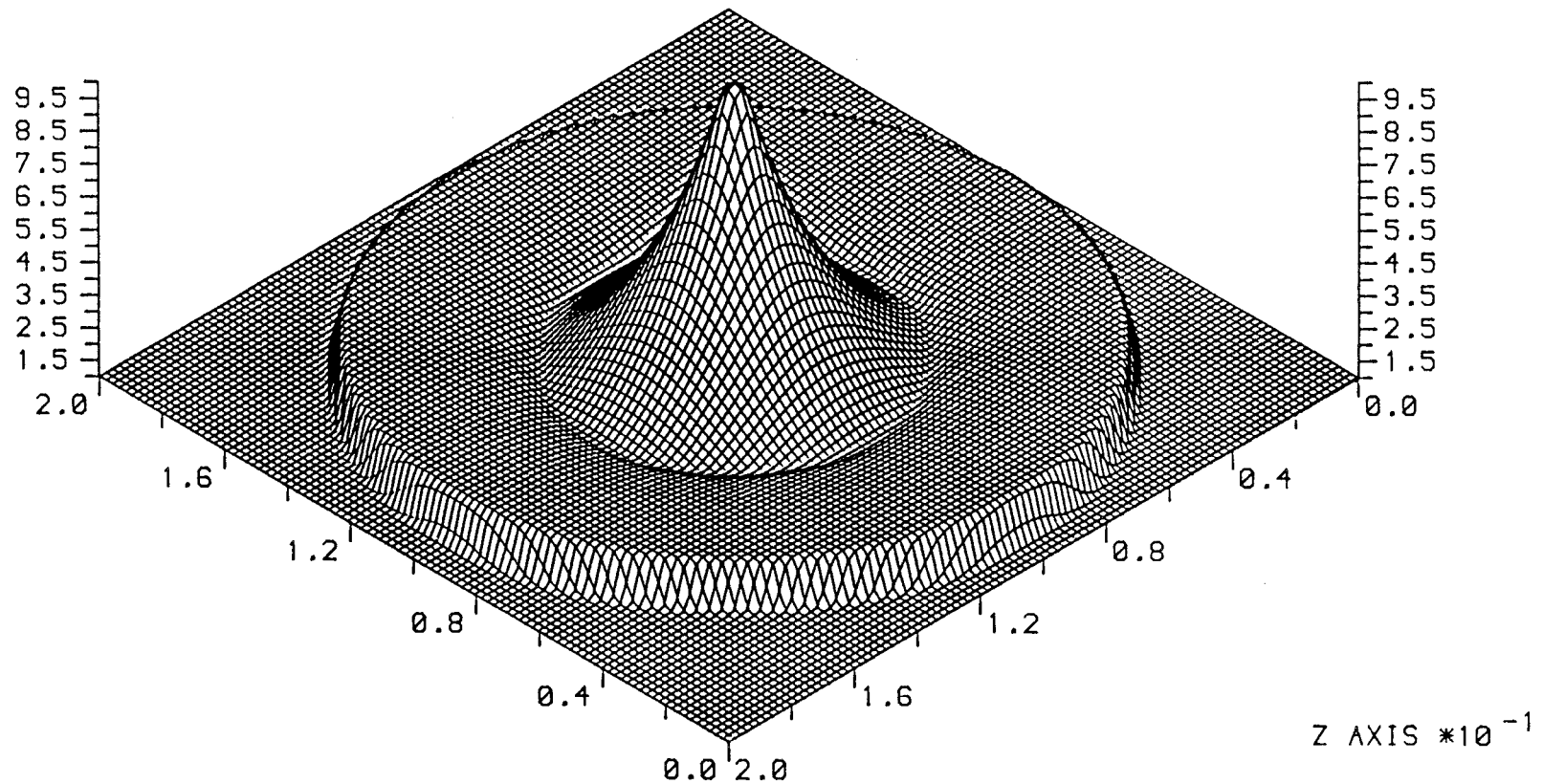
9.5
8.5
7.5
6.5
5.5
4.5
3.5
2.5
1.5
2.0
1.6
1.2
0.8
0.4
0.0
2.0
1.6
1.2
0.8
0.4
0.0
9.5
8.5
7.5
6.5
5.5
4.5
3.5
2.5
1.5
0.0
Z AXIS *10 -1

(17)

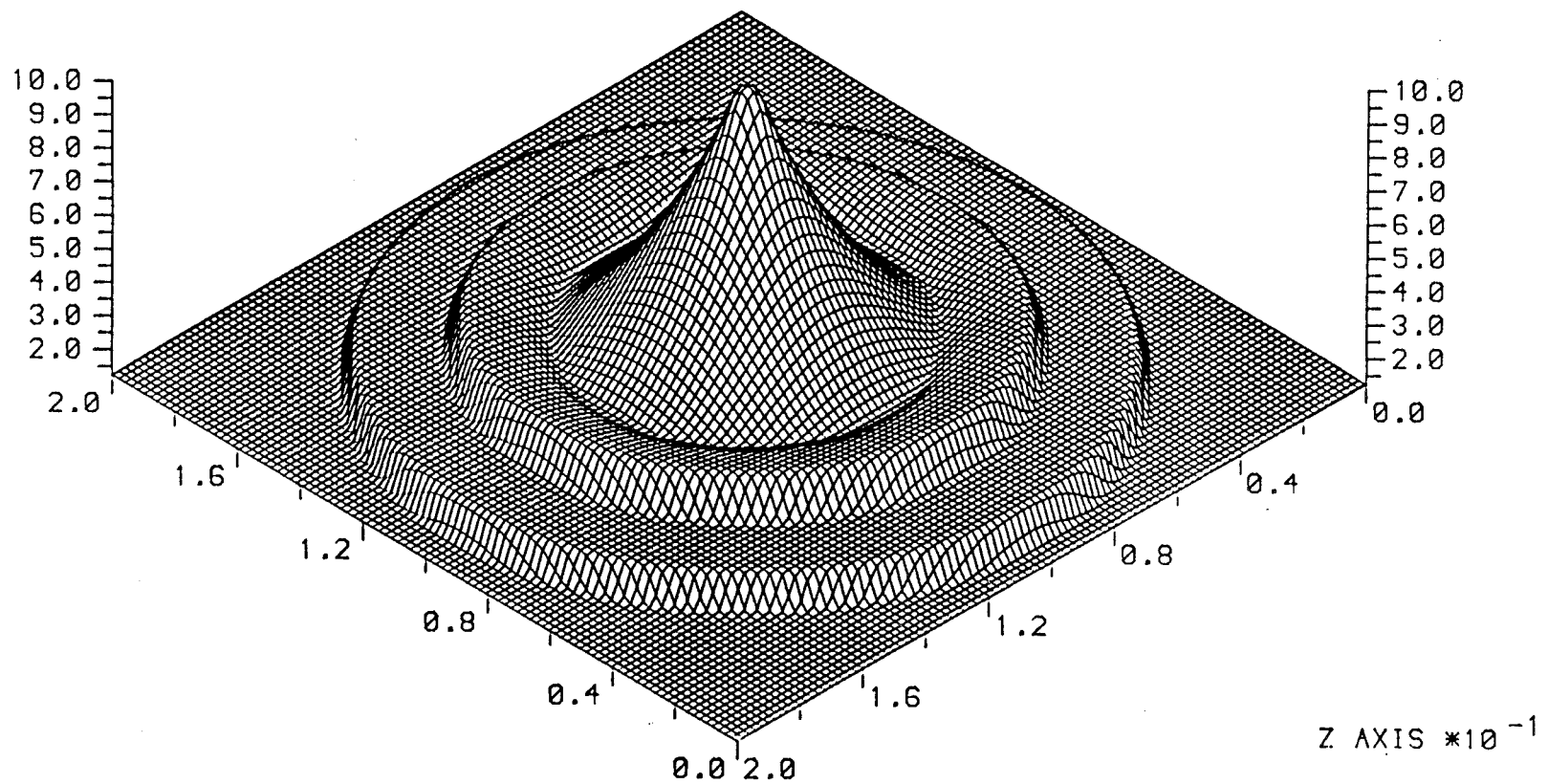
10.0
9.0
8.0
7.0
6.0
5.0
4.0
3.0
2.0
2.0
1.6
1.2
0.8
0.4
0.0
2.0
1.6
1.2
0.8
0.4
0.0
10.0
9.0
8.0
7.0
6.0
5.0
4.0
3.0
2.0
0.0
Z AXIS *10 -1

(18)

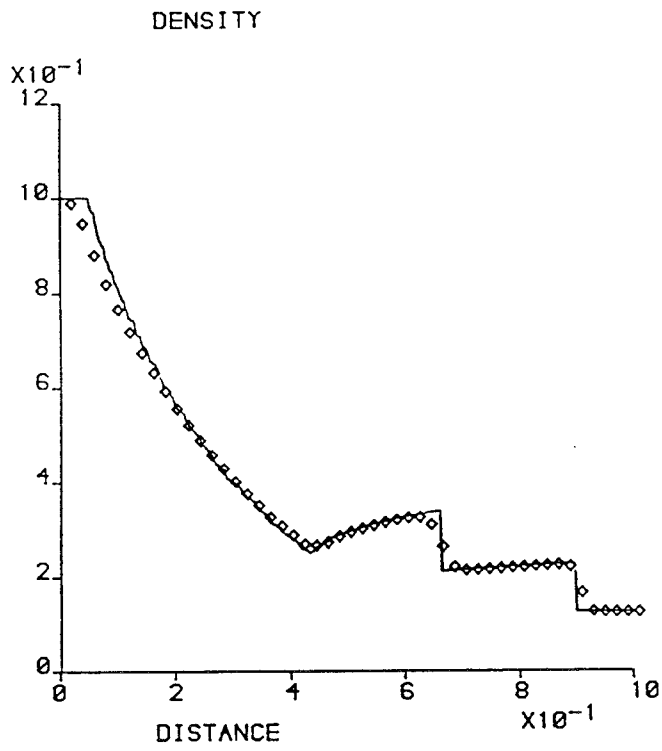
DENSITY
X10⁻¹
12
10
8
6
4
2
0
0
2
4
6
8
10
X10⁻¹
DISTANCE

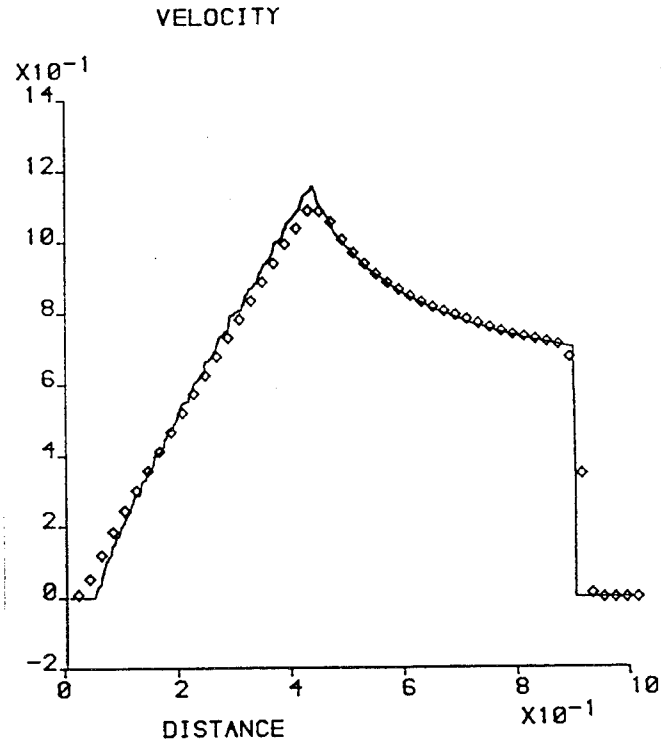
VELOCITY
X10⁻¹
14
12
10
8
6
4
2
0
-2
0
2
4
6
8
10
X10⁻¹
DISTANCE

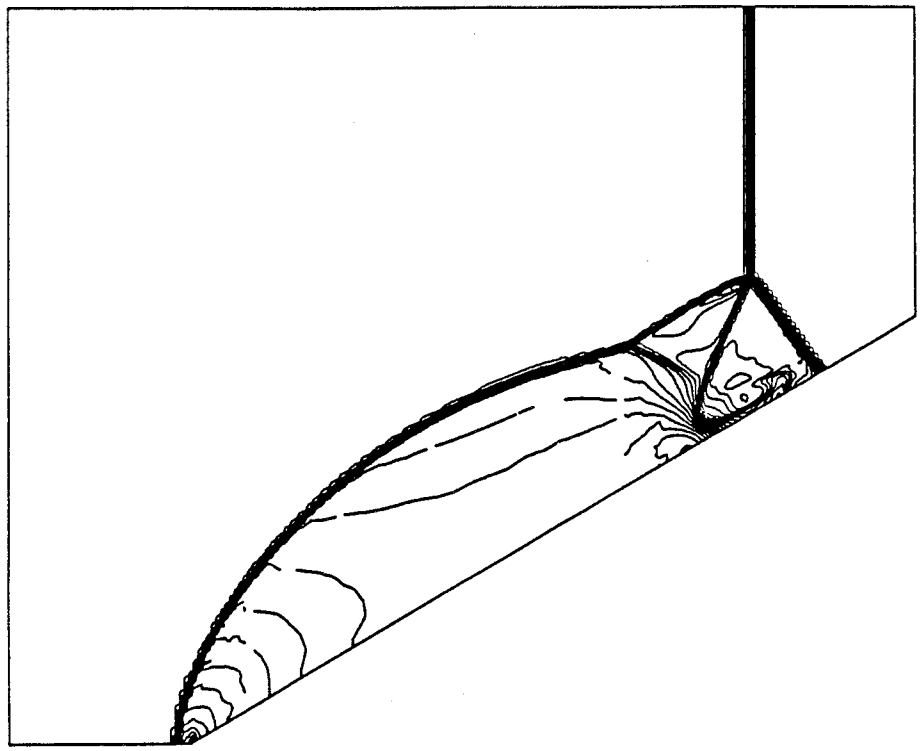

20

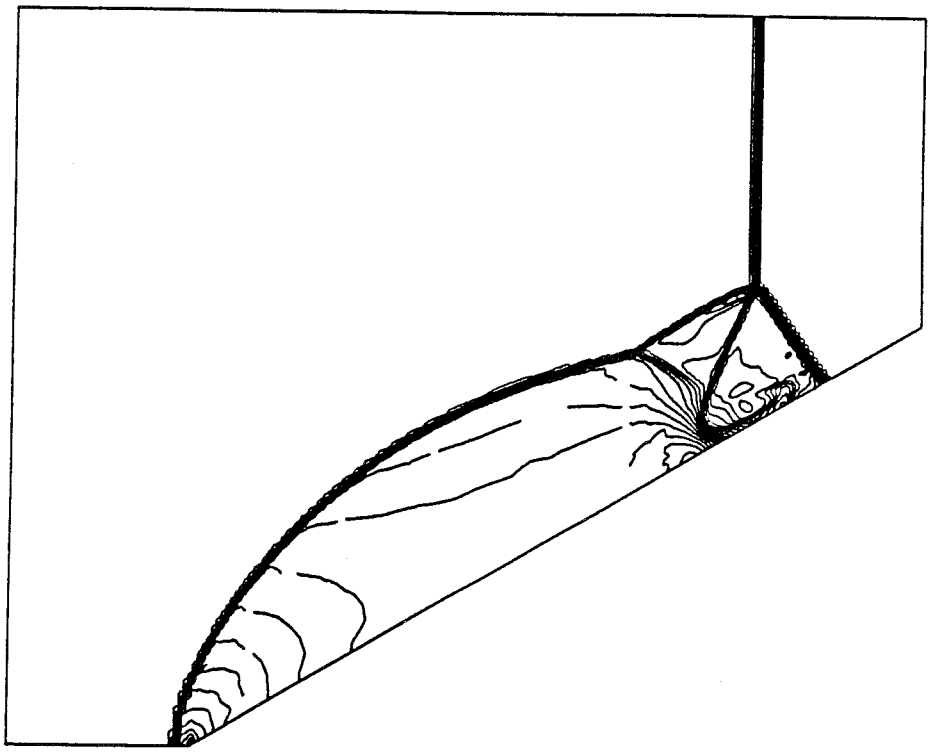

Exact Riemann Solver